Structural, Spectroscopic, and Theoretical Characterization of Bis(μ-oxo)dicopper Complexes, Novel Intermediates in Copper-Mediated Dioxygen Activation

Samiran Mahapatra, Jason A. Halfen, Elizabeth C. Wilkinson, Gaofeng Pan, Xuedong Wang, Victor G. Young, Jr., Christopher J. Cramer,* Lawrence Que, Jr.,* and William B. Tolman*

Contribution from the Department of Chemistry, Center for Metals in Biocatalysis, and Supercomputer Institute, University of Minnesota, 207 Pleasant St. SE, Minneapolis, Minnesota 55455

Received July 5, 1996[⊗]

Abstract: A description of the structure and bonding of novel bis(μ-oxo)dicopper complexes and their bis(μ-hydroxo)-dicopper decomposition products was derived from combined X-ray crystallographic, spectroscopic, and *ab initio* theoretical studies. The compounds $[(LCu)_2(\mu\text{-}O)_2]X_2$ were generated from the reaction of solutions of [LCu-(CH_3CN)]X with O_2 at −80 °C (L = 1,4,7-tribenzyl-1,4,7-triazacyclononane, L^{Bn_3}; 1,4,7-triisopropyl-1,4,7-triazacyclononane, L^{iPr_3}; or 1-benzyl-4,7-diisopropyl-1,4,7-triazacyclononane, L^{iPr_2Bn}; X = variety of anions). The geometry of the $[Cu_2(\mu\text{-}O)_2]^{2+}$ core was defined by X-ray crystallography for $[(d_{21}\text{-}L^{Bn_3}Cu)_2(\mu\text{-}O)_2](SbF_6)_2$ and by EXAFS spectroscopy for the complexes capped by L^{Bn_3} and L^{iPr_3}; notable dimensions include short Cu−O (∼1.80 Å) and Cu···Cu (∼2.80 Å) distances like those reported for analogous $M_2(\mu\text{-}O)_2$ (M = Fe or Mn) rhombs. The core geometry is contracted compared to those of the bis(μ-hydroxo)dicopper(II) compounds that result from decomposition of the bis(μ-oxo) complexes upon warming. X-ray structures of the decomposition products $[(L^{Bn_3}Cu)(L^{Bn_2H}Cu)(\mu\text{-}OH)_2](O_3SCF_3)_2\cdot 2CH_3CO$, $[(L^{iPr_2H}Cu)_2(\mu\text{-}OH)_2](BPh_4)_2\cdot 2THF$, and $[(L^{iPr_2Bn}Cu)_2(\mu\text{-}OH)_2](O_3SCF_3)_2$ showed that they arise from N-dealkylation of the original capping macrocycles. Manometric, electrospray mass spectrometric, and UV−vis, EPR, NMR, and resonance Raman spectroscopic data for the bis(μ-oxo)dicopper complexes in solution revealed important topological and electronic structural features of the intact $[Cu_2(\mu\text{-}O)_2]^{2+}$ core. The bis(μ-oxo)-dicopper unit is diamagnetic, undergoes a rapid fluxional process involving interchange of equatorial and axial N-donor ligand environments, and exhibits a diagnostic ∼600 cm^{-1} ^{18}O-sensitive feature in Raman spectra. *Ab initio* calculations on a model system, $\{[(NH_3)_3Cu]_2(\mu\text{-}O)_2\}^{2+}$, predicted a closed-shell singlet ground-state structure that agrees well with the bis(μ-oxo)dicopper geometry determined by experiment and helps to rationalize many of its physicochemical properties. On the basis of an analysis of the theoretical and experimental results (including a bond valence sum analysis), a formal oxidation level assignment for the core is suggested to be $[Cu^{III}_2(\mu\text{-}O^{2-})_2]^{2+}$, although a more complete molecular orbital description indicates that the oxygen and copper fragment orbitals are significantly mixed (i.e., there is a high degree of covalency).

The binding and activation of dioxygen by copper ions is important in numerous and diverse biological and catalytic processes.[1] Biomolecules having one or more copper ions in their active sites utilize the oxidizing power of O_2 for respiration and for the functionalization of diverse substrates during metabolically significant biochemical pathways. Copper−dioxygen interactions also play a central role in synthetically useful stoichiometric and catalytic oxidative conversions of organic molecules. Thus, an important research objective that has attracted the attention of an interdisciplinary community of scientists is to elucidate the nature and reactivity of copper−dioxygen adducts.[1,2]

The few such Cu_n-O_2 units in synthetic compounds that have been structurally characterized by X-ray crystallography are shown in Figure 1;[3,4] alternative binding modes have been suggested for additional complexes based on spectroscopic and kinetic data.[5] A representative demonstration of the successful interplay of direct biophysical studies and synthetic modeling work is the development of the now coherent picture of the reversible binding of O_2 to hemocyanin (Hc), the dioxygen carrier protein found in arthropods and mollusks. In Hc, two Cu(I) ions, each ligated by three histidyl imidazoles, form a

* To whom correspondence should be addressed. E-mail: cramer@umn.edu, que@chem.umn.edu, and tolman@chem.umn.edu. FAX: 612-624-7029.

[⊗] Abstract published in *Advance ACS Abstracts*, November 1, 1996.

(1) For reviews, see: (a) Karlin, K. D.; Gultneh, Y. *Prog. Inorg. Chem.* **1987**, *35*, 219−328. (b) Sorrell, T. N. *Tetrahedron* **1989**, *40*, 3−68. (c) Karlin, K. D.; Tyeklár, Z.; Zuberbühler, A. D. In *Bioinorganic Catalysis*; Reedjik, J., Ed.; Marcel Dekker, Inc.: New York, 1993; pp 261−315. (d) Kitajima, N.; Moro-oka, Y. *Chem. Rev.* **1994**, *94*, 737. (e) Karlin, K. D.; Tyeklár, Z. *Adv. Inorg. Biochem.* **1994**, *9*, 123−172. (f) Fox, S.; Karlin, K. D. In *Active Oxygen in Biochemistry*; Valentine, J. S., Foote, C. S., Greenberg, A., Liebman, J. F., Eds.; Blackie Academic & Professional, Chapman & Hall: Glasgow, Scotland, 1995; pp 188−231.

(2) (a) Solomon, E. I.; Baldwin, M. J.; Lowery, M. D. *Chem. Rev.* **1992**, *92*, 521−542. (b) Solomon, E. I.; Tuczek, F.; Root, D. E.; Brown, C. A. *Chem. Rev.* **1994**, *94*, 827−856.

(3) (a) Tyeklár, Z.; Jacobson, R. R.; Wei, N.; Murthy, N. N.; Zubieta, J.; Karlin, K. D. *J. Am. Chem. Soc.* **1993**, *115*, 2677−2689. (b) Kitajima, N.; Fujisawa, K.; Fujimoto, C.; Moro-oka, Y.; Hashimoto, S.; Kitagawa, T.; Toriumi, K.; Tatsumi, K.; Nakamura, A. *J. Am. Chem. Soc.* **1992**, *114*, 1277−1291. (c) Fujisawa, K.; Tanaka, M.; Moro-oka, Y.; Kitajima, N. *J. Am. Chem. Soc.* **1994**, *116*, 12079−12080. (d) Reim, J.; Krebs, B. *Angew. Chem., Int. Ed. Engl.* **1994**, *33*, 1969−1971.

(4) An X-ray crystal structure of a complex comprised of an (η^1-superoxo)copper(II) unit stabilized by hydrogen bonding interactions with ligand amide groups has been reported,[4a] but the X-ray data were incorrectly interpreted. A subsequent reanalysis of the data showed the molecule to contain a terminal hydroxide rather than a superoxide ligand.[4b] (a) Harata, M.; Jitsukawa, K.; Masuda, H.; Einaga, H. *J. Am. Chem. Soc.* **1994**, *116*, 10817−10818. (b) Berreau, L.; Mahapatra, S.; Halfen, J. A.; Young, V. G., Jr.; Tolman, W. B. *Inorg. Chem.* **1996**, *35*, 6339−6342.

S0002-7863(96)02305-0 CCC: $12.00

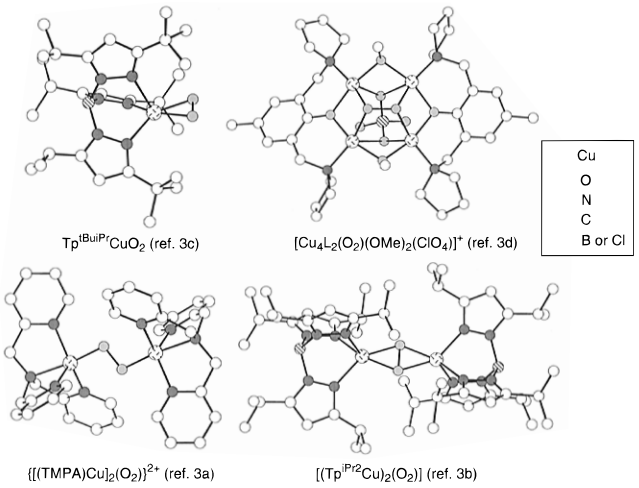

Figure 1. Chem3D representations of the existing X-ray structures of copper−dioxygen adducts.

dioxygen adduct (oxyHc) having a planar (μ-η^2:η^2-peroxo)-dicopper(II) core. The geometric features of this $[Cu_2(\mu\text{-}\eta^2\text{:}\eta^2\text{-}O_2)]^{2+}$ unit have been defined by X-ray crystallography in oxyHc[6] and, in greater detail, in the synthetic model complex $[(Tp^{iPr_2}Cu)_2(O_2)]$ [Tp^{iPr_2} = tris(3,5-diisopropyl-1-pyrazolyl)-hydroborate] (Figure 1).[3b] Diagnostic spectroscopic features of this core include EPR silence due to strong antiferromagnetic coupling between the Cu(II) ions, a low O−O stretching frequency in the resonance Raman spectrum [$\sim$750 cm^{-1}; $\Delta\nu(^{18}O_2)$ = 42 cm^{-1}], and peroxo → Cu(II) charge transfer bands in the optical absorption spectrum [λ_{max} = 360 (ϵ 20 000 M^{-1} cm^{-1}), 510 (ϵ 1000) nm].[2,7] Since its characterization in $[(Tp^{iPr_2}Cu)_2(O_2)]$ and oxyHc, the $[Cu_2(\mu\text{-}\eta^2\text{:}\eta^2\text{-}O_2)]^{2+}$ fragment has been indentified in a number of other complexes, all with facially coordinating, tridentate N-donor capping ligands.[8,9] Moreover, reversible O_2 binding behavior that was not observed for the Tp^{iPr_2} complex has been demonstrated in these instances.

The physicochemical characterization data for the copper−dioxygen adducts shown in Figure 1 in conjunction with comprehensive kinetic and thermodynamic data for the formation of these and other complexes[5,10] has provided considerable insight into the first steps involved in dioxygen binding and activation. Nonetheless, many important issues remain unresolved, in particular the nature of the subsequent O−O bond cleavage that invariably occurs in oxidation reactions. Whether O−O bond disruption occurs prior to or concomitant with attack on substrate is another key question. In contrast to the situation for other metal-promoted oxidations, such as those involving heme-iron sites,[11] understanding of these issues has been inhibited by a dearth of definitively identified intermediates beyond the Cu_n-O_2 (n = 1 or 2) adduct stage. In synthetic chemistry, oxygenation of Cu(I) complexes commonly occurs with a 4:1 Cu:O_2 reaction stoichiometry to yield oxo- or hydroxocopper(II) products.[12] These products generally are believed to arise via formation of a (peroxo)dicopper(II) intermediate that is induced to undergo O−O bond cleavage by the additional Cu(I) ions, which act as sources of electrons (eq 1). Although examples of structurally characterized bis-

$$2Cu^{I} + O_2 \rightarrow Cu^{II}-(O_2^{2})-Cu^{II} \xrightarrow{2Cu^{I}} 2Cu^{II}-O(H)-Cu^{II} \quad (1)$$

(μ-hydroxo)dicopper(II) are numerous,[13] only a few high nuclearity oxocopper(II) clusters[14] and discrete oxodicopper-(II) species have been identified,[12c,15,16] and crystallographically characterized examples exist only for species comprised of more than two copper ions.

Increasingly oxidized species resulting from O−O bond cleavage without further injection of electrons from additional Cu(I) ions have been even more elusive, yet they are key intermediates in proposed mechanisms of oxidative transformations carried out by copper-containing enzymes or synthetic catalysts.[17,18] For example, Klinman and co-workers have suggested that in dopamine β-monooxygenase a tyrosine residue and a nearby monocopper hydroperoxide [Cu(II)−OOH] react

(5) Some selected examples: (a) Karlin, K. D.; Tyeklár, Z.; Farooq, A.; Haka, M. S.; Ghosh, P.; Cruse, R. W.; Gultneh, Y.; Hayes, J. C.; Toscano, P. J.; Zubieta, J. *Inorg. Chem.* **1992**, *31*, 1436−1451. (b) Sanyal, I.; Strange, R. W.; Blackburn, N. J.; Karlin, K. D. *J. Am. Chem. Soc.* **1991**, *113*, 4692−4693. (c) Karlin, K. D.; Wei, N.; Jung, B.; Kaderli, S.; Niklaus, P.; Zuberbühler, A. D. *J. Am. Chem. Soc.* **1993**, *115*, 9506−9514. (d) Jung, B.; Karlin, K. D.; Zuberbühler, A. D. *J. Am. Chem. Soc.* **1996**, *118*, 3763−3764.

(6) (a) Magnus, K. A.; Hazes, B.; Ton-That, H.; Bonaventura, C.; Bonaventura, J.; Hol, W. G. J. *Proteins: Struct., Funct., Genet.* **1994**, *19*, 302−309. (b) Magnus, K. A.; Ton-That, H.; Carpenter, J. E. *Chem. Rev.* **1994**, *94*, 727−735.

(7) Baldwin, M. J.; Root, D. E.; Pate, J. E.; Fujisawa, K.; Kitajima, N.; Solomon, E. I. *J. Am. Chem. Soc.* **1992**, *114*, 10421−10431.

(8) (a) Lynch, W. E.; Kurtz, D. M., Jr.; Wang, S.; Scott, R. A. *J. Am. Chem. Soc.* **1994**, *116*, 11030−11038. (b) Sorrell, T. N.; Allen, W. E.; White, P. S. *Inorg. Chem.* **1995**, *34*, 952−960.

(9) Mahapatra, S.; Halfen, J. A.; Wilkinson, E. C.; Que, L., Jr.; Tolman, W. B. *J. Am. Chem. Soc.* **1994**, *116*, 9785−9786.

(10) (a) Wei, N.; Lee, D.-H.; Murthy, N. N.; Tyeklár, Z.; Karlin, K. D.; Kaderli, S.; Jung, B.; Zuberbühler, A. D. *Inorg. Chem.* **1994**, *33*, 4625−4626. (b) Cruse, R. W.; Kaderli, S.; Karlin, K. D.; Zuberbuhler, A. D. *J. Am. Chem. Soc.* **1988**, *110*, 6882−6883. (c) Karlin, K. D.; Wei, N.; Jung, B.; Kaderli, S.; Zuberbühler, A. D. *J. Am. Chem. Soc.* **1991**, *113*, 5868−5870.

(11) *Cytochrome P-450: Structure, Mechanism, and Biochemistry*, 2nd ed.; Ortiz de Montellano, P. R., Ed.; Plenum Press: New York, 1995.

(12) (a) Davies, G.; El-Sayed, M. A. *Comments Inorg. Chem.* **1985**, *4*, 151−162. (b) Davies, G.; El-Sayed, M. A. *Inorg. Chem.* **1983**, *22*, 1257−1266. (c) Caulton, K. G.; Davies, G.; Holt, E. M. *Polyhedron* **1990**, *9*, 2319−2351 and references cited therein. (d) Sanyal, I.; Mahroof-Tahir, M.; Nasir, M. S.; Ghosh, P.; Cohen, B. I.; Gultneh, Y.; Cruse, R. W.; Farooq, A.; Karlin, K. D.; Liu, S.; Zubieta, J. *Inorg. Chem.* **1992**, *31*, 4322−4332. (e) Lee, D.-H.; Murthy, N. N.; Karlin, K. D. *Inorg. Chem.* **1996**, *35*, 804−805 and references cited therein.

(13) (a) Lee, S. C.; Holm, R. H. *Inorg. Chem.* **1993**, *32*, 4745−4753 and references cited therein. (b) Hodgson, D. J. *Prog. Inorg. Chem.* **1975**, *19*, 173−242. (c) Kitajima, N.; Hikichi, S.; Tanaka, M.; Moro-oka, Y. *J. Am. Chem. Soc.* **1993**, *115*, 5496−5508.

(14) (a) Ross, P. F.; Murmann, R. K.; Schlemper, E. O. *Acta Crystallogr.* **1974**, *B30*, 1120−1123. (b) Butcher, R. J.; O'Connor, C. J.; Sinn, E. *Inorg. Chem.* **1981**, *20*, 537−545. (c) Erdonmez, A.; van Diemen, J. H.; de Graaff, R. A. G.; Reedjik, J. *Acta Crystallogr.* **1990**, *C46*, 402−404. (d) McKee, V.; Tandon, S. S. *J. Chem. Soc., Dalton Trans.* **1991**, 221−230. (e) Agnus, Y.; Louis, R.; Metz, B.; Boudon, C.; Gisselbrecht, J. P.; Gross, M. *Inorg. Chem.* **1991**, *30*, 3155−3161 and references cited therein. (f) Davies, G.; El-Shazly, M. F.; Rupich, M. W.; Churchill, M. R.; Rotella, R. J. *J. Chem. Soc., Chem. Commun.* **1978**, 1045−1046. (g) Hosokawa, T.; Takano, M.; Murahashi, S.-I. *J. Am. Chem. Soc.* **1996**, *118*, 3990−3991.

(15) (a) Lapinte, C.; Riviere, H.; Roselli, A. *J. Chem. Soc., Chem. Commun.* **1981**, 1109−1110. (b) Kitajima, N.; Koda, T.; Moro-oka, Y. *Chem. Lett.* **1988**, 347−350.

(16) Kitajima, N.; Koda, T.; Iwata, Y.; Moro-oka, Y. *J. Am. Chem. Soc.* **1990**, *112*, 8833−8839.

(17) Some examples where the involvement of Cu(III)═O ↔ Cu(II)−O$^{\bullet}$ or related high oxidation state species have been suggested: (a) Villafranca, J. J. In *Copper Proteins*; Spiro, T. G., Ed.; Wiley: New York, 1981; pp 264−289. (b) Capdevielle, P.; Baranne-Lafont, J.; Sparfel, D.; Cuong, N. K.; Maumy, M. *J. Mol. Catal.* **1988**, *47*, 59−66. (c) Réglier, M.; Amadeï, E.; Tadayoni, R.; Waegell, B. *J. Chem. Soc., Chem. Commun.* **1989**, 447−450. (d) Capdevielle, P.; Sparfel, D.; Baranne-Lafont, J.; Cuong, N. K.; Maumy, M. *J. Chem. Soc., Chem. Commun.* **1990**, 565−566. (e) Reinaud, O.; Capdevielle, P.; Maumy, M. *J. Chem. Soc., Chem. Commun.* **1990**, 566−568. (f) Capdevielle, P.; Maumy, M. *Tetrahedron Lett.* **1991**, *32*, 3831−3834. (g) Reddy, K. V.; Jin, S.-J.; Arora, P. K.; Sfeir, D. S.; Maloney, S. C. F.; Urbach, F. L.; Sayre, L. M. *J. Am. Chem. Soc.* **1990**, *112*, 2332−2340 and references cited therein. (h) Itoh, S.; Kondo, T.; Komatsu, M.; Ohshiro, Y.; Li, C.; Kanehisa, N.; Kai, Y.; Fukuzumi, S. *J. Am. Chem. Soc.* **1995**, *117*, 4714−4715. (i) Chan, S. I.; Nguyen, H.-H. T.; Shiemke, A. K.; Lidstrom, M. E. In *Bioinorganic Chemistry of Copper*; Karlin, K. D., Tyeklár, Z., Eds.; Chapman & Hall: New York, 1993; pp 184−195. (j) Ogura, T.; Hirota, S.; Proshlyakov, D. A.; Shinzawa-Itoh, K.; Yoshikawa, S.; Kitagawa, T. *J. Am. Chem. Soc.* **1996**, *118*, 5443−5449.

(18) Tian, G.; Berry, J. A.; Klinman, J. P. *Biochemistry* **1994**, *33*, 226−234.

to generate a tyrosyl radical and a mono(oxocopper) unit [often written as Cu(III)═O ↔ Cu(II)−O•, although the former is untenable][19] that abstracts a benzylic hydrogen atom from substrate during the catalytic mechanism.[18] On the basis of kinetic investigations, analogous $Tp^{Me_2}CuO$ fragments were postulated to form upon cleavage of $[(Tp^{Me_2}Cu)_2(\mu\text{-}\eta^2\text{:}\eta^2\text{-}O_2)]$ in the rate-determining step of its decomposition,[16] but structural or spectroscopic support for such a mono(oxocopper) species in this or other synthetic or biological systems is notably absent. The only oxocopper(III) species to be structurally characterized appear in the solid state chemical literature;[20] these include $MCuO_2$ (M = group IA alkali metal),[21] $SrLaCuO_4$,[22] and $Na_3Cu_2O_3$.[21,23] Electrochemical oxidation of oxotricopper(II) species has been reported to yield mixed-valent (μ-oxo)tricopper(II,II,III) complexes,[24] but these have not been definitively characterized by X-ray structural methods nor have they been generated from O_2.

We recently discovered that solutions of $[L^{iPr_3}Cu(CH_3CN)]O_3SCF_3$ (L^{iPr_3} = 1,4,7-triisopropyl-1,4,7-triazacyclononane)[25] in CH_2Cl_2 at −80 °C bind O_2 reversibly to form a $(\mu\text{-}\eta^2\text{:}\eta^2$-peroxo)dicopper(II) species analogous to oxyHc.[9] By performing the oxygenation reaction in THF or by starting with a Cu(I) complex of 1,4,7-tribenzyl-1,4,7-triazaclononane (L^{Bn_3})[26] instead of L^{iPr_3} in a variety of solvents, new species with spectroscopic properties different from those associated with the $[Cu_2(\mu\text{-}\eta^2\text{:}\eta^2\text{-}O_2)]^{2+}$ unit were obtained.[27,28] We have identified these new species as having previously unobserved $[Cu_2(\mu\text{-}O)_2]^{2+}$ cores [formally bis(μ-oxo)dicopper(III)], akin to analogous rhombs containing iron(III and/or IV)[29] or manganese(III and/or IV)[30] ions. Such high oxidation state "diamond-like" cores are becoming recognized as important entities in a number of processes carried out by multinuclear metalloprotein active sites,[31] including those that feature dioxygen activation (methane monooxygenase,[32] ribonucleotide reductase)[33] and generation (oxygen evolving complex in photosystem II).[34] Indeed, the potential involvement of such cores in both types of processes has been placed on firmer ground by our discovery that the $[Cu_2(\mu\text{-}O)_2]^{2+}$ and the $[Cu_2(\mu\text{-}\eta^2\text{:}\eta^2\text{-}O_2)]^{2+}$ species can interconvert, and that they both decompose to bis(μ-hydroxo)dicopper(II) species by pathways involving rate-determining cleavage of ligand substituent C−H bonds.[27,28]

Stimulated by its novelty and its relevance to biological oxidations and catalysis, we have endeavored to fully characterize the novel $[Cu_2(\mu\text{-}O)_2]^{2+}$ core by structural, spectroscopic, and theoretical methods. Herein we provide a full description of the results of these studies, which have utilized X-ray crystallography, EXAFS, UV−vis absorption, NMR, and resonance Raman spectroscopies, electrospray mass spectrometry, bond valence sum analysis, and *ab initio* calculations to understand the structure and bonding of the bis(μ-oxo)dicopper complexes. For comparative purposes, we also describe the nature of various bis(μ-hydroxo)dicopper(II) complexes having N-dealkylated ligands that are produced upon decomposition of the title compounds. Studies of the mechanism by which the bis(μ-oxo)dicopper complexes undergo ligand N-dealkylation via C−H bond activation are presented separately.[35]

Results and Discussion

Syntheses. The Cu(I) starting materials $[LCu(CH_3CN)]X$ [L = L^{Bn_3} or 1-benzyl-4,7-diisopropyl-1,4,7-triazacyclononane (L^{iPr_2Bn}), X = ClO_4^-, $O_3SCF_3^-$, or SbF_6^-; L = L^{iPr_3}, X = ClO_4^-, PF_6^-, BPh_4^-, SbF_6^-, $O_3SCF_3^-$, or $B(Ar_f)_4^-$][36] were prepared in straightforward fashion, either by mixing the macrocycle L with $[Cu(CH_3CN)_4]X$ according to a published procedure[37] or by a subsequent anion exchange to further vary X. The ligand L^{iPr_2Bn} is new; it was prepared by benzylation of 1,4-diisopropyl-1,4,7-triazacyclononane,[38] which was constructed in turn from 1-tosyl-1,4,7-triazacyclononane[39] through alkylation with isopropyl bromide followed by a final detosylation (see the Experimental Section). All Cu(I) complexes were isolated as air-sensitive colorless or pale yellow solids and were characterized by NMR and IR spectroscopy and elemental analysis. The anticipated trend in electron donating abilities $L^{iPr_3} > L^{iPr_2Bn} > L^{Bn_3}$ was confirmed by comparison of the ν(CO) of derived $[LCuCO]^+$ adducts prepared by treating representative complexes with 1 atm CO; ν(CO) = 2067, 2069, and 2084 cm^{-1}, respectively. Although distinguishable by IR spectroscopy, the differences in electron donating characteristics of the three ligands are not large, as is shown by the only slightly differing $E_{1/2}$ values in their cyclic voltammograms [$E_{1/2}$ (ΔE_p) = 360 (110), 415 (170), and 420 (310) mV vs SCE in CH_3CN with 0.2 M Bu_4NPF_6 at a scan rate of 100 mV s^{-1}, respectively].

Bubbling O_2 through colorless to pale yellow solutions of $[L^{Bn_3}Cu(CH_3CN)]X$ or $[L^{iPr_2Bn}Cu(CH_3CN)]X$ (X = ClO_4^-, $O_3SCF_3^-$, or SbF_6^-) in CH_2Cl_2, acetone, or THF at −80 °C induced a color change to deep orange-brown that we attribute to the formation of the respective bis(μ-oxo)dicopper complexes $[(LCu)_2(\mu\text{-}O)_2](X)_2$ (L = L^{Bn_3} or L^{iPr_2Bn}, Scheme 1). The optical absorbance spectra of these deeply colored solutions contain

(19) Mayer, J. M. *Comments Inorg. Chem.* **1988**, *8*, 125−135.
(20) Levason, W.; Spicer, M. D. *Coord. Chem. Rev.* **1987**, *76*, 45−120.
(21) Hestermann, K.; Hoppe, R. *Z. Anorg. Allg. Chem.* **1969**, *367*, 249−280.
(22) Goodenough, J. B.; Demazeau, G.; Pouchard, M.; Hagenmuller, P. *J. Solid State Chem.* **1973**, *8*, 325−330.
(23) A tricopper(II,II,III) cluster capped by O atoms derived from O_2 and bonded to the Cu(III) ion at short (∼1.83 Å) distances was reported recently: (a) Cole, A. P.; Root, D. E.; Solomon, E. I.; Stack, T. D. P. *Abstracts of Papers*, 211th National Meeting of the American Chemical Society, New Orleans, LA; American Chemical Society: Washington, DC, 1996; INORG 060. (b) Cole, A. P.; Root, D. E.; Solomon, E. I.; Stack, T. D. P. *Science* **1996**, *273*, 1848−1850.
(24) (a) Datta, D.; Mascharak, P. K.; Chakravorty, A. *Inorg. Chem.* **1981**, *20*, 1673−1679. (b) Datta, D.; Chakravorty, A. *Inorg. Chem.* **1982**, *21*, 363−368. (c) Datta, D.; Chakravorty, A. *Inorg. Chem.* **1983**, *22*, 1611−1613.
(25) Haselhorst, G.; Stoetzel, S.; Strassburger, A.; Walz, W.; Wieghardt, K.; Nuber, B. *J. Chem. Soc., Dalton Trans.* **1993**, 83−90.
(26) Beissel, T.; Della Vedova, B. S. P. C.; Wieghardt, K.; Boese, R. *Inorg. Chem.* **1990**, *29*, 1736−1741.
(27) Mahapatra, S.; Halfen, J. A.; Wilkinson, E. C.; Pan, G.; Cramer, C. J.; Que, L., Jr.; Tolman, W. B. *J. Am. Chem. Soc.* **1995**, *117*, 8865−8866.
(28) Halfen, J. A.; Mahapatra, S.; Wilkinson, E. C.; Kaderli, S.; Young, V. G., Jr.; Que, L., Jr.; Zuberbühler, A. D.; Tolman, W. B. *Science* **1996**, *271*, 1397−1400.
(29) (a) Zang, Y.; Dong, Y.; Que, L., Jr.; Kauffmann, K.; Münck, E. *J. Am. Chem. Soc.* **1995**, *117*, 1169−1170. (b) Dong, Y.; Fujii, H.; Hendrich, M. P.; Leising, R. A.; Pan, G.; Randall, C. R.; Wilkinson, E. C.; Zang, Y.; Que, L., Jr.; Fox, B. G.; Kauffmann, K.; Münck, E. *J. Am. Chem. Soc.* **1995**, *117*, 2778−2792.
(30) (a) Wieghardt, K. *Angew. Chem., Int. Ed. Engl.* **1989**, *28*, 1153−1172. (b) Manchanda, R.; Brudvig, G. W.; Crabtree, R. H. *Coord. Chem. Rev.* **1995**, *144*, 1−38.
(31) Que, L., Jr.; Dong, Y. *Acc. Chem. Res.* **1996**, *29*, 190−196.
(32) (a) Lipscomb, J. D. *Annu. Rev. Microbiol.* **1994**, *48*, 371−399. (b) Wallar, B. J.; Lipscomb, J. D. *Chem. Rev.*, in press.
(33) (a) Stubbe, J. *Adv. Enzymol.* **1990**, *63*, 349−419. (b) Fontecave, M.; Nordlund, P.; Eklund, H.; Reichard, P. *Adv. Enzymol.* **1992**, *65*, 147−183. (c) Sturgeon, B. E.; Burdi, D.; Chen, S.; Huynh, B.-H.; Edmondson, D. E.; Stubbe, J.; Hoffman, B. M. *J. Am. Chem. Soc.* **1996**, *118*, 7551−7557.
(34) Sauer, K.; Yachandra, V. K.; Britt, R. D.; Klein, M. P. In *Manganese Redox Enzymes*; Pecoraro, V. L., Ed.; VCH: New York, 1992; pp 141−175.
(35) Mahapatra, S.; Halfen, J. A.; Tolman, W. B. *J. Am. Chem. Soc.* **1996**, *118*, 11575−11586.
(36) $B(Ar_f)_4^- = B[3,5\text{-}(CF_3)_2C_6H_3]_4^-$; Brookhart, M.; Grant, B.; Volpe, A. F., Jr. *Organometallics* **1992**, *11*, 3920−3922.
(37) Halfen, J. A.; Mahapatra, S.; Wilkinson, E. C.; Gengenbach, A. J.; Young, V. G., Jr.; Que, L., Jr.; Tolman, W. B. *J. Am. Chem. Soc.* **1996**, *118*, 763−776.
(38) Houser, R. P.; Halfen, J. A.; Young, V. G., Jr.; Blackburn, N. J.; Tolman, W. B. *J. Am. Chem. Soc.* **1995**, *117*, 10745−10746.
(39) Sessler, J. L.; Sibert, J. W.; Lynch, V. *Inorg. Chem.* **1990**, *29*, 4143−4146.

Scheme 1

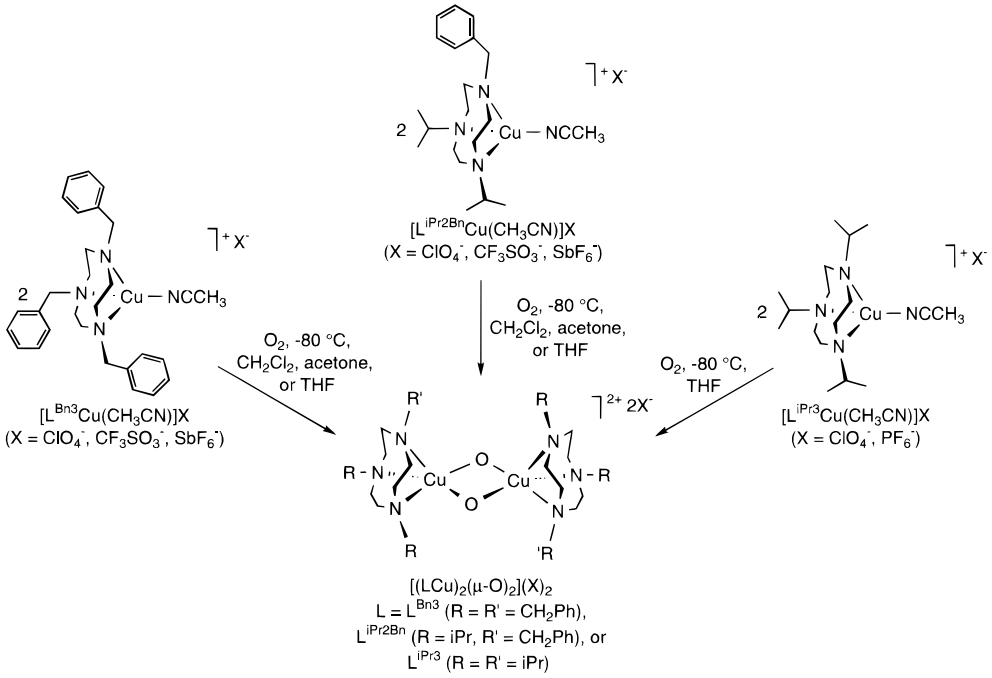

Table 1. Spectroscopic Properties of Bis(μ-oxo)dicopper Complexes

complex	manometry Cu:O_2	UV−vis[a] λ_{max}, nm (ϵ, M^{-1} cm^{-1})	resonance Raman[b] $\nu_{Cu_2O_2}$, cm^{-1}	NMR[c] δ, ppm
$[(L^{Bn_3}Cu)_2(\mu\text{-}O)_2](ClO_4)_2$	2.2(2):1	430 (14 000), 318 (12 000)	602, 612 (583)	^{1}H (500 MHz): 7.37 (s, 10H), 7.29 (s, 20H), 4.59 (s, 12H), 3.48 (s, 12H), 2.55 (s, 12H). $^{13}C\{^1H\}$ (125 MHz): 133.0, 132.3, 128.9, 59.5, 51.6 (br)
$[(L^{iPr_3}Cu)_2(\mu\text{-}O)_2](ClO_4)_2$	2.0(2):1	448 (13 000), 324 (11 000)	600 (580)	
$[(L^{iPr_2Bn}Cu)_2(\mu\text{-}O)_2](ClO_4)_2$	2.0(2):1	436 (16 000), 322 (12 000)	594 (572)	

[a] Measured in either CH_2Cl_2 (L^{Bn_3} and L^{iPr_2Bn}) or THF (L^{iPr_3}) at −80 °C. [b] The resonance Raman spectra were obtained at 77 K as frozen CH_2Cl_2 or THF solutions using 457 nm laser excitation; only ^{18}O sensitive vibrations are quoted with specific ^{18}O shifts in parentheses. [c] Recorded in 1:2 $CD_2Cl_2/(CD_3)_2CO$ solvent mixture at −75 °C.

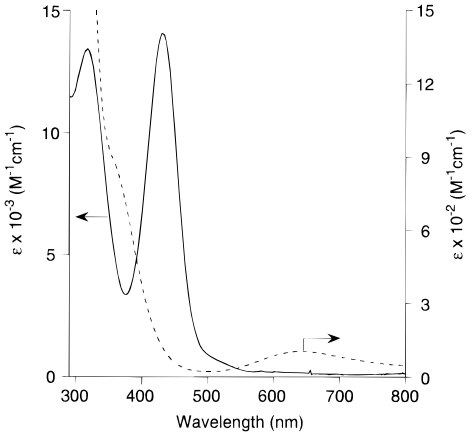

Figure 2. UV−vis spectrum of $[(L^{Bn_3}Cu)_2(\mu\text{-}O)_2](SbF_6)_2$ in CH_2Cl_2 at −80 °C (-) and of the solution resulting upon its decomposition (- - -).

two intense, presumably charge transfer bands with $\lambda_{max} \cong 320$ nm (ϵ 12 000 M^{-1} cm^{-1} per dicopper complex) and 430 nm (ϵ 14 000 M^{-1} cm^{-1}) (Table 1 and Figure 2). These features vary little among the species generated with the two macrocyclic coligands L^{Bn_3} or L^{iPr_2Bn} or the various counterions or solvents. They are distinct from the absorption bands characteristic for the planar (μ-η^2:η^2-peroxo)dicopper(II) core.[3b,8,9] The oxygenation reaction of $[L^{iPr_3}Cu(CH_3CN)]X$ [X = ClO_4^-, PF_6^-, BPh_4^-, SbF_6^-, $O_3SCF_3^-$, or $B(Ar_f)_4^-$] is more complicated, since either bis(μ-oxo)- or (μ-η^2:η^2-peroxo)dicopper species or both are generated depending on the solvent and/or counterion used as shown by UV−vis and/or resonance Raman (vide infra) spectroscopic monitoring. For example, in CH_2Cl_2 for all counterions (X) the predominant (>90%) product is $[(L^{iPr_3}Cu)_2(\mu\text{-}\eta^2\text{:}\eta^2\text{-}O_2)](X)_2$, in THF or acetone with X = BPh_4^-, SbF_6^-, $O_3SCF_3^-$, and/or $B(Ar_f)_4^-$ both species are present [~4:1 peroxo:bis(μ-oxo) ratio], and in THF with X = ClO_4^- or PF_6^- only $[(L^{iPr_3}Cu)_2(\mu\text{-}O)_2](X)_2$ forms. A detailed analysis of this evidently complex influence of solvent and counterion on the nature and interconversion of these oxygenation products will be the subject of a future report. Importantly in the current context, solutions resulting from oxygenation of $[L^{iPr_3}Cu(CH_3CN)]X$ (X = ClO_4^- or PF_6^-) in THF exhibit UV−vis absorption features nearly identical to those observed when L = L^{Bn_3} or L^{iPr_2Bn} (Table 1), demonstrating the clean generation of analogous bis(μ-oxo)dicopper cores and no μ-η^2:η^2-peroxo isomers in each case.

Dinuclear formulations for the complexes in solution were supported by manometric measurements of O_2 uptake and, in one instance, electrospray mass spectrometry.[40] Manometry experiments (3−5 replicate runs) for the reaction of O_2 with $[LCu(CH_3CN)]ClO_4$ (L = L^{Bn_3} or L^{iPr_2Bn}) in CH_2Cl_2 and with $[L^{iPr_3}Cu(CH_3CN)]ClO_4$ in THF at −80 °C indicated Cu:O_2 stoichiometries of 2:1 (Table 1). Electrospray mass spectra were obtained for solutions of $[(d_{21}\text{-}L^{Bn_3}Cu)_2(\mu\text{-}O)_2](X)_2$ (X = SbF_6^- or ClO_4^-), perdeuterated at the ligand alkyl substituents in order to enhance stability (vide infra), in CH_2Cl_2 at ca. −40 °C. We observed parent ion envelopes with isotope patterns consistent

(40) Kim, J.; Dong, Y.; Larka, E.; Que, L., Jr. *Inorg. Chem.* **1996**, *35*, 2369−2372.

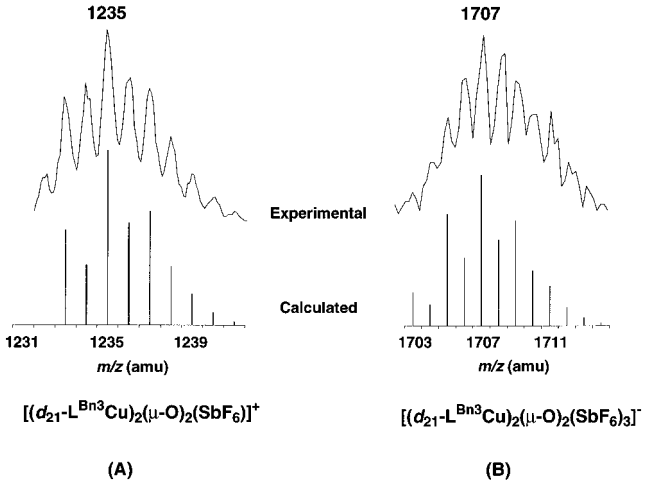

Figure 3. Experimental (top) and calculated (bottom) peak envelopes in the positive ion (A) and negative ion (B) electrospray mass spectra of $[(d_{21}\text{-}L^{Bn_3}Cu)_2(\mu\text{-}O)_2](SbF_6)_2$ in CH_2Cl_2.

with the indicated formulations; exemplary positive and negative ion mass spectra and simulations for the respective parent ions $\{[(d_{21}\text{-}L^{Bn_3}Cu)_2(\mu\text{-}O)_2]SbF_6\}^+$ and $\{[(d_{21}\text{-}L^{Bn_3}Cu)_2(\mu\text{-}O)_2](SbF_6)_3\}^-$ are shown in Figure 3. Electrospray data for hydroxo-bridged decomposition products contain parent ion envelopes of similar shape, but, as expected, are shifted 2 *m/z* units higher.

The bis(μ-oxo)dicopper complexes are unstable in solution and in the solid state, as evidenced by a change in color from orange-brown to green that is accompanied by a loss of the intense CT absorption bands associated with the $[Cu_2(\mu\text{-}O)_2]^{2+}$ core (Figure 1). The decomposition rates were significantly slowed by using ligands with deuterated substituents on the triazacyclononane ligands; a detailed discussion of these kinetic isotope effects and the mechanism of decomposition is presented elsewhere.[35] Various bis(μ-hydroxo)dicopper(II) complexes with differing capping ligands were isolated from the green decomposed solutions (Scheme 2), three of which were structurally characterized by X-ray crystallography (vide infra). As shown in Scheme 2, either the symmetric species $[(L^{Bn_3}Cu)_2(\mu\text{-}OH)_2]^{2+}$ or the unsymmetric compound $[(L^{Bn_3}Cu)(L^{Bn_2H}Cu)(\mu\text{-}OH)_2]^{2+}$ having a singly N-dealkylated capping ligand was crystallized from the solution resulting from decomposition of $[(L^{Bn_3}Cu)_2(\mu\text{-}O)_2]^{2+}$, the identity of the isolated product being dependent on the counterion used (ClO_4^- or $CF_3SO_3^-$, respectively) and the crystallization conditions. The products isolated from the decompositions of $[(LCu)_2(\mu\text{-}O)_2](ClO_4)_2$ (L = L^{iPr_3} or L^{iPr_2Bn}) were $[(L^{iPr_2H}Cu)_2(\mu\text{-}OH)_2](BPh_4)_2$, in which only N-dealkylated caps are present, or $[(L^{iPr_2Bn}Cu)_2(\mu\text{-}OH)_2](O_3SCF_3)_2$, with unperturbed substituents, respectively (the different counterions were introduced via metathesis after completion of the decomposition). The isolated yields of the various products were variable and in no instance were we able to conclusively identify all copper-containing species after the decomposition reactions. We suspect that, for each case, the green decomposed solutions contain rapidly interconverting statistical mixtures of bis(hydroxo)dicopper(II) complexes with two intact, one intact and one dealkylated, or two dealkylated ligands and that the specific counterion and crystallization conditions dictate which dinuclear species crystallizes.

In order to substantiate the hypothesis that the bis(hydroxo) compounds equilibrate in solution, we performed a simple cross-over experiment. Electrospray mass spectrometric analysis of the solution obtained by mixing equimolar solutions of $[(L^{Bn_3}Cu)_2(\mu\text{-}OH)_2](SbF_6)_2$ and $[(d_{21}\text{-}L^{Bn_3}Cu)_2(\mu\text{-}OH)_2](SbF_6)_2$ in CH_2Cl_2 at room temperature for 30 min indicated the presence of a 1:2:1 ratio of $\{[(L^{Bn_3}Cu)_2(\mu\text{-}OH)_2](SbF_6)\}^+$ (M^+ envelope at *m/z* ~1197), $\{[(L^{Bn_3}Cu)(d_{21}\text{-}L^{Bn_3}Cu)(\mu\text{-}OH)_2](SbF_6)\}^+$ (M^+ at *m/z* ~1218), and $\{[(d_{21}\text{-}L^{Bn_3}Cu)_2(\mu\text{-}OH)_2](SbF_6)\}^+$ (M^+ at *m/z* ~1239). The observation of this statistical mixture supports equilibration among the various hydroxo-bridged complexes in solution, presumably via a bridge cleavage/recombination process(es) that would be expected to be more facile than alternatives involving dissociation/reassociation of the capping macrocyclic ligands.

X-ray Crystallography. Crystallographic data and selected bond distances and angles for the X-ray structures of $[(d_{21}$-

Scheme 2

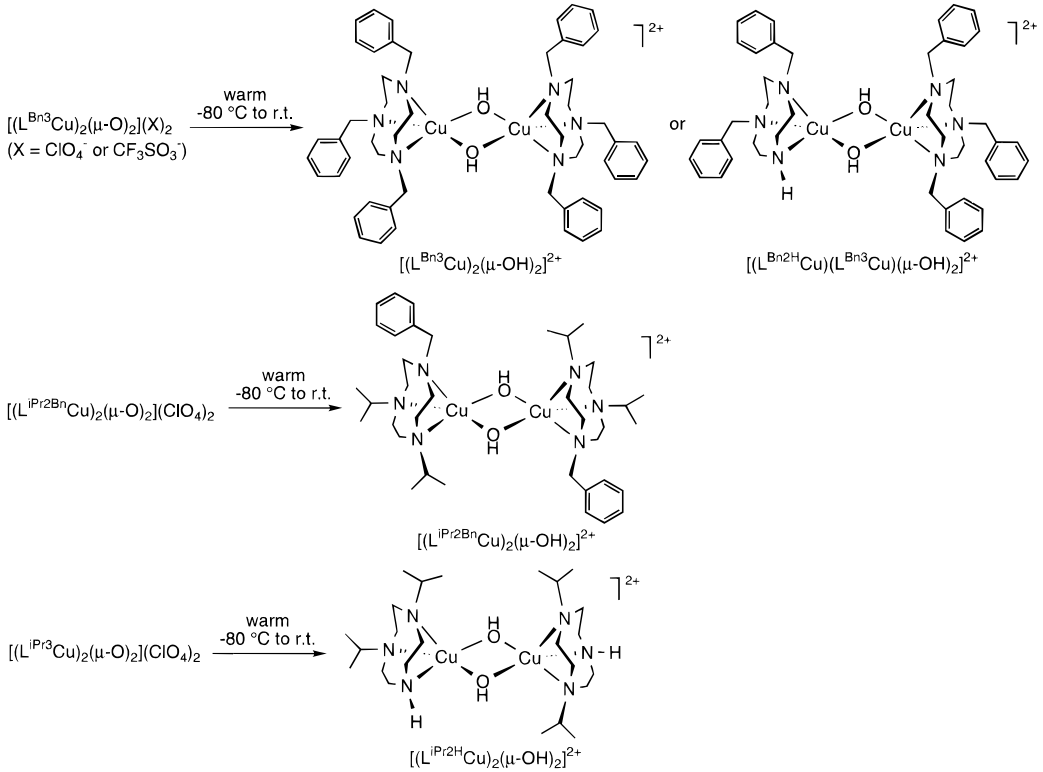

Table 2. Summary of X-ray Crystallographic Data

	$[(d_{21}\text{-}L^{Bn_3}Cu)_2(\mu\text{-}O)_2](SbF_6)_2\cdot 7(CH_3)_2CO\cdot 2CH_3CN$	$[(L^{Bn_3}Cu)(L^{Bn_2H}Cu)(\mu\text{-}OH)_2](CF_3SO_3)_2\cdot 2(CH_3)_2CO$	$[(L^{iPr_2H}Cu)_2(\mu\text{-}OH)_2](BPh_4)_2\cdot 2THF$	$[(L^{iPr_2Bn}Cu)_2(\mu\text{-}OH)_2](CF_3SO_3)_2$
emp form	$C_{79}H_{72}D_{42}F_{12}Cu_2N_8O_9Sb_2$	$C_{55}H_{74}F_6Cu_2N_6O_{10}S_2$	$C_{80}H_{112}B_2Cu_2N_6O_4$	$C_{40}H_{68}F_6Cu_2N_6O_8S_2$
fw	1960.70	1284.4	1370.46	1066.21
cryst syst	monoclinic	monoclinic	monoclinic	monoclinic
space group	*C*2/*c*	$P2_1/n$	*Cc*	$P2_1/a$ (no. 14)
a (Å)	26.1916(6)	15.1315(2)	23.7906(4)	21.326(7)
b (Å)	15.3560(4)	26.0344(4)	16.7455(4)	10.887(2)
c (Å)	22.2705(6)	15.3733(3)	21.7924(2)	23.316(8)
β (deg)	96.493(1)	92.788(1)	120.462(1)	113.36(1)
V (Å^3)	8899.7(4)	6049.0(2)	7483.4(2)	4970(5)
Z	8	4	4	4
density(calcd) (mg/cm^3)	1.462	1.410	1.216	1.425
temp (K)	123(2)	173(2)	173(2)	297(2)
crystal size (mm)	0.50 × 0.38 × 0.30	0.35 × 0.30 × 0.15	0.40 × 0.24 × 0.04	0.36 × 0.24 × 0.15
diffractometer	Siemens SMART	Siemens SMART	Siemens SMART	Enraf-Nonius CAD-4
radiation	Mo Kα (0.710 73 Å)	Mo Kα (0.710 73 Å)	Mo Kα (0.710 73 Å)	Mo Kα (0.710 73 Å)
absn coeff	1.153 mm^{-1}	0.850 mm^{-1}	0.621 mm^{-1}	10.11 cm^{-1}
2θ max (deg)	50.32	48.22	48.14	50.1
no. of reflns colld	22487	24233	15400	9499
no. of ind reflns	7865	9409	10282	9237
no. of obsd reflns [$I > 2\sigma(I)$]	6599	6822	8393	3528
params	523	801	856	577
$R1^a$ [$I > 2\sigma(I)$]	0.1012	0.077	0.0824	0.069
Rw^a				0.058
$wR2^b$	0.2532	0.1585	0.1797	
goodness-of-fit	1.051	1.091	1.142	1.41
largest diff peak and hole (e$^-$ Å^{-3})	2.941, −2.38[c]	0.947, −0.661	0.568, −0.557	0.56, −0.66

[a] $R1 = \sum||F_o| - |F_c||/\sum|F_o|$; $Rw = [(\sum w(|F_o| - |F_c|)^2/\sum wF_o^2)]^{1/2}$, where $w = 4F_o^2/\sigma^2(F_o^2)$, $\sigma^2(F_o^2) = [S^2(C + R^2B) + (pF_o^2)^2]/Lp^2$, S = scan rate, C = total integrated peak count, R = ratio of scan time to background counting time, B = total background count, Lp = Lorentz-polarization factor, and p = p-factor. [b] $wR2 = [\sum[w(F_o^2 - F_c^2)^2]/\sum[w(F_o^2)^2]]^{1/2}$, where $w = 1/\sigma^2(F_o^2) + (aP)^2 + bP$. [c] Located near disordered SbF_6^- anion.

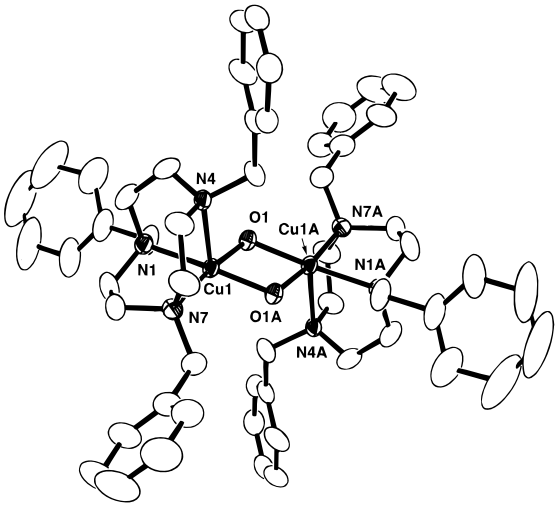

Figure 4. Representation of the dication in the X-ray crystal structure of $[(d_{21}\text{-}L^{Bn_3}Cu)_2(\mu\text{-}O)_2](SbF_6)_2\cdot 7(CH_3)_2CO\cdot 2CH_3CN$ (35% ellipsoids, hydrogen and deuterium atoms omitted for clarity).

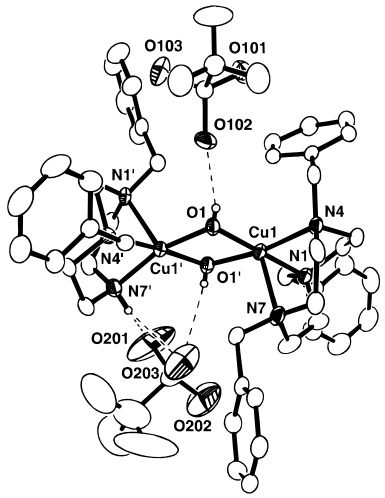

Figure 5. Representation of the X-ray crystal structure of $[(L^{Bn_3}Cu)(L^{Bn_2H}Cu)(\mu\text{-}OH)_2](O_3SCF_3)_2\cdot 2(CH_3)_2CO$ (35% ellipsoids, acetone solvate and all hydrogen atoms except those bonded to N or O omitted for clarity, dashed lines indicate postulated hydrogen bonds).

$L^{Bn_3}Cu)_2(\mu\text{-}O)_2](SbF_6)_2\cdot 7(CH_3)_2CO\cdot 2CH_3CN$ and the bis(μ-hydroxo)dicopper(II) complexes $[(L^{Bn_3}Cu)(L^{Bn_2H}Cu)(\mu\text{-}OH)_2](O_3SCF_3)_2\cdot 2CH_3CO$, $[(L^{iPr_2H}Cu)_2(\mu\text{-}OH)_2](BPh_4)_2\cdot 2THF$, and $[(L^{iPr_2Bn}Cu)_2(\mu\text{-}OH)_2](O_3SCF_3)_2$ are summarized in Tables 2 and 3, with drawings shown in Figures 4−8 {only one of the two independent but chemically similar molecules in the asymmetric unit of $[(L^{iPr_2Bn}Cu)_2(\mu\text{-}OH)_2](O_3SCF_3)_2$ is shown}. Complete listings of positional parameters, temperature factors, and bond distances and angles for all of the compounds are provided as supporting information. We discuss the structures of the bis(μ-hydroxo)dicopper(II) complexes first in order to more readily draw comparisons of their cores with that of the unique bis(μ-oxo) compound.

Bis(μ-hydroxo)dicopper(II) Complexes. Examination of the molecular structures of the three bis(μ-hydroxo)dicoppper(II) complexes shown in Figures 5−7 reveals similar core geometries typical for this molecular motif,[13] but with different capping ligands and hydrogen-bonding patterns. The hydroxo bridges occupy equatorial coordination sites in all three structures, with average parameters Cu−O = 1.94 Å [range 1.921(5)−1.975(6) Å], Cu−O−Cu = 101.5° [range 100.5(2)−102.9(3)°], and Cu···Cu = 3.01 Å [range 2.9769(9)−3.037(3) Å]. The copper ions in each complex have slightly distorted square pyramidal coordination geometries; the axial N-donors are disposed *anti* with respect to the $[Cu_2(\mu\text{-}OH)_2]^{2+}$ core. While the original macrocyclic ligand is retained intact in $[(L^{iPr_2Bn}Cu)_2(\mu\text{-}OH)_2](O_3SCF_3)_2$ (Figure 7), the occurrence of N-dealkylation chemistry upon decomposition of the respective bis(μ-oxo)dicopper precursors supported by L^{Bn_3} or L^{iPr_3} is evident from the structures shown in Figures 5 and 6, which contain either one or two N−H instead of N−R groups (R =

Table 3. Selected Bond Lengths (Å) and Angles (deg) for Complexes Characterized by X-ray Crystallography[a]

$[(d_{21}\text{-}L^{Bn_3}Cu)_2(\mu\text{-}O)_2](SbF_6)_2\cdot 7(CH_3)_2CO\cdot 2CH_3CN$			
Cu(1)−O(1)	1.803(5)	Cu(1)−O(1A)	1.808(5)
Cu(1)−N(1)	1.987(6)	Cu(1)−N(4)	2.298(6)
Cu(1)−N(7)	1.986(6)	O(1)−Cu(1)−O(1A)	78.6(2)
Cu(1)···Cu(1A)	2.794(2)	O(1)−Cu(1)−N(1)	172.3(2)
O(1)−Cu(1)−N(4)	102.3(2)	O(1)−Cu(1)−N(7)	96.2(2)
O(1A)−Cu(1)−N(1)	95.6(2)	O(1A)−Cu(1)−N(4)	103.8(2)
O(1A)−Cu(1)−N(7)	171.1(2)	Cu(1)−O(1)−Cu(1A)	101.4(2)
$[(L^{Bn_3}Cu)(L^{Bn_2H}Cu)(\mu\text{-}OH)_2](CF_3SO_3)_2\cdot 2(CH_3)_2CO$			
Cu(1)−O(1)	1.949(4)	Cu(1)−O(1′)	1.924(5)
Cu(1)−N(1)	2.087(5)	Cu(1)−N(4)	2.054(4)
Cu(1)−N(7)	2.289(5)	Cu(1′)−O(1)	1.921(5)
Cu(1′)−O(1′)	1.940(4)	Cu(1′)−N(1′)	2.266(5)
Cu(1′)−N(4′)	2.085(5)	Cu(1′)−N(7′)	2.029(5)
Cu(1)···Cu(1′)	2.9769(9)	O(1)−Cu(1)−O(1′)	78.6(2)
O(1)−Cu(1)−N(1)	176.2(2)	O(1)−Cu(1)−N(4)	97.7(2)
O(1)−Cu(1)−N(7)	99.1(2)	O(1′)−Cu(1)−N(1)	98.3(2)
O(1′)−Cu(1)−N(4)	170.4(2)	O(1′)−Cu(1)−N(7)	106.1(2)
O(1′)−Cu(1′)−O(1)	78.9(2)	O(1′)−Cu(1′)−N(1′)	112.9(2)
O(1′)−Cu(1′)−N(4′)	175.1(2)	O(1′)−Cu(1′)−N(7′)	94.9(2)
Cu(1)−O(1)−Cu(1′)	100.5(2)	Cu(1)−O(1′)−Cu(1′)	100.8(2)
$[(L^{iPr_2H}Cu)_2(\mu\text{-}OH)_2](BPh_4)_2\cdot 2THF$			
Cu(1)−O(1)	1.922(6)	Cu(1)−O(2)	1.951(6)
Cu(1)−N(11)	2.017(8)	Cu(1)−N(14)	2.303(7)
Cu(1)−N(17)	2.086(8)	Cu(2)−O(1)	1.930(6)
Cu(2)−O(2)	1.951(6)	Cu(2)−N(21)	2.008(9)
Cu(2)−N(24)	2.335(9)	Cu(2)−N(27)	2.048(8)
Cu(1)···Cu(2)	3.0088(13)	O(1)−Cu(1)−O(2)	78.3(3)
O(1)−Cu(1)−N(14)	115.8(3)	O(1)−Cu(1)−N(11)	161.2(3)
O(1)−Cu(2)−N(21)	93.7(3)	O(1)−Cu(1)−N(17)	100.1(3)
O(2)−Cu(1)−N(11)	96.5(3)	O(1)−Cu(2)−N(27)	168.2(3)
O(2)−Cu(2)−N(17)	175.8(3)	O(2)−Cu(1)−N(14)	99.3(3)
O(2)−Cu(2)−N(24)	107.6(3)	O(2)−Cu(2)−N(21)	169.1(3)
O(1)−Cu(1)−Cu(2)	38.7(2)	O(2)−Cu(2)−N(27)	101.7(3)
O(1)−Cu(2)−Cu(1)	38.6(2)	O(1)−Cu(1)−O(2)	78.1(2)
O(2)−Cu(2)−Cu(1)	39.6(2)	O(2)−Cu(1)−Cu(2)	39.5(2)
Cu(2)−O(2)−Cu(1)	100.9(3)	Cu(1)−O(1)−Cu(2)	102.7(3)
$[(L^{iPr_2Bn}Cu)_2(\mu\text{-}OH)_2](CF_3SO_3)_2$			
Molecule 1			
Cu(1)−O(1)	1.950(6)	Cu(1)−O(1′)	1.933(6)
Cu(1)−N(1)	2.113(8)	Cu(1)−N(4)	2.065(8)
Cu(1)−N(7)	2.260(8)	Cu(1)···Cu(1′)	3.037(3)
O(1)−Cu(1)−O(1′)	77.1(3)	O(1)−Cu(1)−N(1)	159.4(3)
O(1)−Cu(1)−N(4)	98.6(3)	O(1)−Cu(1)−N(7)	117.1(3)
O(1′)−Cu(1)−N(1)	98.0(3)	O(1′)−Cu(1)−N(4)	173.6(3)
O(1′)−Cu(1)−N(7)	101.1(3)	Cu(1)−O(1)−Cu(1′)	102.9(3)
Molecule 2			
Cu(2)−O(2)	1.975(6)	Cu(2)−O(2′)	1.947(6)
Cu(2)−N(11)	2.090(7)	Cu(2)−N(14)	2.053(8)
Cu(2)−N(17)	2.266(8)	Cu(2)···Cu(2′)	3.033(3)
O(2)−Cu(2)−O(2′)	78.7(3)	O(2)−Cu(2)−N(11)	162.7(3)
O(2)−Cu(2)−N(14)	97.4(3)	O(2)−Cu(2)−N(17)	113.2(3)
O(2′)−Cu(2)−N(11)	97.0(3)	O(2′)−Cu(2)−N(14)	173.0(3)
O(2′)−Cu(2)−N(17)	102.2(3)	Cu(2)−O(2)−Cu(2′)	101.3(3)

[a] Estimated standard deviations are given in parentheses.

isopropyl or benzyl). In $[(L^{Bn_3}Cu)(L^{Bn_2H}Cu)(\mu\text{-}OH)_2](O_3SCF_3)_2\cdot 2(CH_3)_2CO$ (Figure 5), the single N−H group and the hydroxide bridges are hydrogen bonded to triflate counterions in the crystal as shown by the dashed lines; relevant distances are O1···O102 = 2.839(5) Å, O1′···O203 = 3.067(5) Å, N7′···O203 = 3.098(5) Å, and N7′···O201 = 3.202(5) Å. The THF solvate molecules in the crystal of $[(L^{iPr_2H}Cu)_2(\mu\text{-}OH)_2](BPh_4)_2\cdot 2THF$ (Figure 6) are hydrogen bonded to the μ-hydroxo groups [O1···O1S = 3.016(8) Å and O2···O2S = 2.930(8) Å], but N−H···X interactions are not evident in this instance. Finally, there are no close contacts between the μ-hydroxo groups and other potential hydrogen bond acceptors in the crystal structure of $[(L^{iPr_2Bn}Cu)_2(\mu\text{-}OH)_2](O_3SCF_3)_2$ (Figure 7). Overall, the three structures exemplify typical $[Cu_2(\mu\text{-}OH)_2]^{2+}$ core geometries[13] and provide unequivocal evidence for N-dealkylation of the

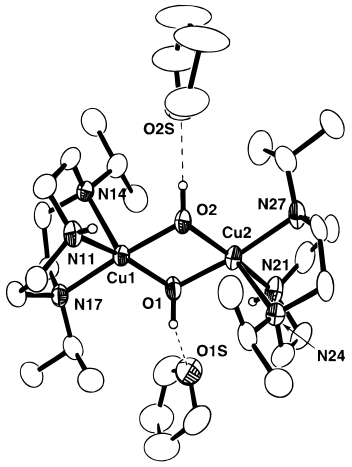

Figure 6. Representation of the dication and the THF solvate molecules in the X-ray crystal structure of $[(L^{iPr_2H}Cu)_2(\mu\text{-}OH)_2](BPh_4)_2\cdot 2THF$ (35% ellipsoids, all hydrogen atoms except those bonded to N or O omitted for clarity, dashed lines indicate postulated hydrogen bonds).

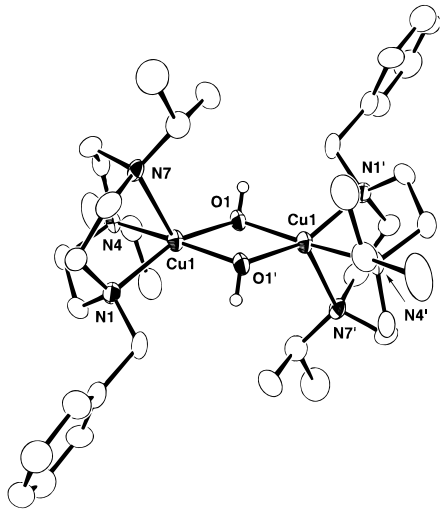

Figure 7. Representation of the dication in the X-ray crystal structure of $[(L^{iPr_2Bn}Cu)_2(\mu\text{-}OH)_2](O_3SCF_3)_2$ (35% ellipsoids, all hydrogen atoms except those bonded to O omitted for clarity).

macrocyclic ligands during decomposition of the bis(μ-oxo)-dicopper precursors.

Bis(μ-oxo)dicopper Complex $[(d_{21}\text{-}L^{Bn_3}Cu)_2(\mu\text{-}O)_2](SbF_6)_2\cdot 7(CH_3)_2CO\cdot 2CH_3CN$. Crystals of this compound suitable for X-ray crystallographic characterization were grown by allowing an oxygenated solution of $[d_{21}\text{-}L^{Bn_3}Cu(CH_3CN)]SbF_6$ in 1:1 $CH_2Cl_2/(CH_3)_2CO$ to stand at −80 °C for 2−3 days, the use of the deuterated ligand $d_{21}\text{-}L^{Bn_3}$ being critical for preventing decomposition of the complex over the time period required for crystallization. As described in detail in the Experimental Section, significant disorder of the SbF_6^- counterion, the solvent molecules, and phenyl groups necessitated imposition of bond distance and anisotropic displacement parameter constraints to force these units to conform to their average respective substructures and to better fit rigid body motion. These aspects of the structure undoubtedly contribute to the relatively high *R* value (10.1%), which nonetheless compares favorably to those reported for other copper−dioxygen complex structures.[3]

A crystallographic inversion center relates the two N_3CuO halves of the novel bis(μ-oxo)dicopper complex (Figure 4). Like the aforementioned bis(μ-hydroxo)dicopper compounds, each copper ion adopts a slightly distorted square pyramidal geometry with the long axial bonds in an *anti* relationship, skewed in this instance by 17° from the axis normal to the equatorial plane. However, the geometrical parameters of the planar $[Cu_2(\mu\text{-}$

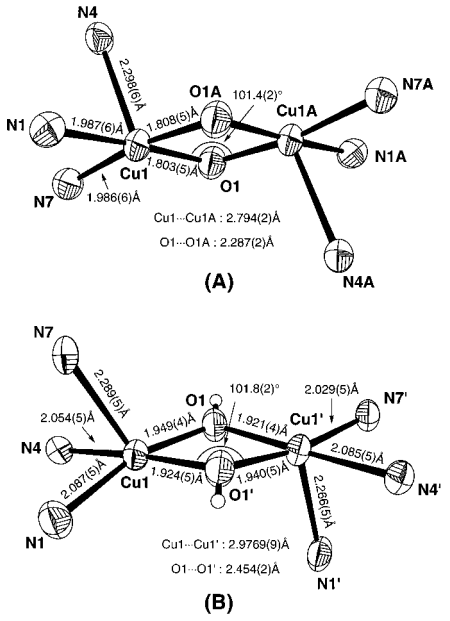

Figure 8. Representation of the copper coordination spheres (50% thermal ellipsoids) in the X-ray crystal structures of (A) $[(d_{21}\text{-}L^{Bn_3}Cu)_2(\mu\text{-}O)_2](SbF_6)_2\cdot 7(CH_3)_2CO\cdot 2CH_3CN$ and (B) $[(L^{Bn_3}Cu)(L^{Bn_2H}Cu)(\mu\text{-}OH)_2](O_3SCF_3)_2\cdot 2(CH_3)_2CO$.

$O)_2]^{2+}$ core differ significantly from those of the isomeric $[Cu_2(\mu\text{-}\eta^2\text{:}\eta^2\text{-}O_2)]^{2+}$ unit in $[(Tp^{iPr_2}Cu)_2(O_2)]$[3b] and those typically observed in $[Cu_2(OH)_2]^{2+}$ cores, as illustrated by the comparision with that of $[(L^{Bn_3}Cu)(L^{Bn_2H}Cu)(\mu\text{-}OH)_2](O_3SCF_3)_2\cdot 2CH_3CO$ in Figure 8. Note that the 2.794(2) Å Cu···Cu and 1.81 Å (av) Cu−O distances in the bis(μ-oxo) compound are significantly shorter than those in the bis(μ-hydroxo) complex [2.9769(9) Å and 1.93 Å (av), respectively]. Interestingly, the Cu−O(H)−Cu angles are essentially identical in the two cores, suggesting that the contracted metal−metal separation in the bis(μ-oxo) complex arises entirely from the shortened Cu−O distances. The Cu···Cu and O···O distances of 2.794(2) and 2.287(5) Å, respectively, for $[(d_{21}\text{-}L^{Bn_3}Cu)_2(\mu\text{-}O)_2](SbF_6)_2$ rule out a possible formulation of the compound as a $\mu\text{-}\eta^2\text{:}\eta^2$-peroxo complex, since the corresponding distances in this latter core are significantly longer and shorter, respectively (3.56 and 1.41 Å).[3b]

Examples of short Cu−O distances in copper(II) coordination chemistry occur in some mononuclear Cu(II)−OH species {Cu−O = 1.875(2) Å in $[Cu(Me_6tren)(OH)]ClO_4$,[41] 1.878(2) Å in $[(tppa)Cu(OH)]ClO_4$},[42] a *trans*-1,2-peroxodicopper(II) complex {Cu−O = 1.852(5) Å in $\{[(TMPA)Cu]_2(O_2)\}(PF_6)_2$},[3a] an oxocopper(II) cluster {Cu−O = 1.85 Å in $[L'_3Cu(O)(ClO_4)]_2$},[43] and in Cu(II)−O−Fe(III) assemblies [1.829(4) Å[41] and 1.856(5) Å[44]]. In these complexes, most of the other Cu−L (L = N or O donor ligand) bond lengths are typical for Cu(II) compounds [~2.0 Å], thus corroborating the +2 formal oxidation levels assigned to the copper ions in each case. In $[(d_{21}\text{-}L^{Bn_3}Cu)_2(\mu\text{-}O)_2](SbF_6)_2$, however, the Cu−O distances are shorter than those noted above and the equatorial Cu−N distances [1.99 Å] also are slightly shorter than those typically found in *bona fide* Cu(II) complexes of triazacyclononane ligands [2.0−2.1 Å]. The observation of this contracted coordination sphere is consistent with assignment of a formal oxidation state greater than +2 to the copper ions.[20] In support of this notion, metal-ligand distances in the few structurally characterized examples of discrete Cu(III) compounds (Table 4, entries 8−13) include a short Cu−O separation of 1.826(3) Å[23,45] and Cu−N distances of 1.80−1.89 Å,[45,46] the latter depending on the nature of the N-donor (amide vs amine). More relevant, perhaps, are the similarities between the core of the bis(oxo) complex and the analogous $Cu_2(\mu\text{-}O)_2$ rhombs present in the oxocopper(III) extended solid $MCuO_2$ (M = group IA alkali metal ion);[21] the Cu−O and Cu···Cu distance and Cu−O−Cu angle parameters of 1.84 Å, 2.71 Å, and 95°, respectively, for $KCuO_2$ compare favorably to the like parameters 1.81 Å, 2.79 Å, and 101° for the bis(oxo) complex.[47] Indeed, the $[Cu_2(\mu\text{-}O)_2]^{2+}$ core geometries in the bis(oxo) complex and $MCuO_2$ closely resemble those of other planar bis(μ-oxo)dimetal units containing iron and manganese in their +3 and/or +4 oxidation states (Table 5),[29,30] thus indicating a general structural uniformity among the different metal-containing cores.

The above qualitative relationship between structural parameters and metal oxidation state can be more quantitatively described through a bond valence sum (BVS) analysis.[48] The BVS for a metal ion is the sum of bond valences s_{ij} for each metal−ligand bond calculated according to eq 2, where r_0 is a

$$\text{BVS} = \sum s_{ij} = \sum \exp[(r_0 - r_{ij})/0.37] \qquad (2)$$

parameter characteristic of that bond and r_{ij} is the experimentally determined bond distance. The empirical r_0 values for many metal−ligand bonds for various metal oxidation states have been determined by averaging r_0 values for sets of like complexes, where each r_0 is calculated by solving eq 2 for r_0 using experimentally determined r_{ij} numbers in complexes of known oxidation state.[48] Using r_0 = 1.679 or 1.719 for Cu(II)−O or Cu(II)−N bonds, respectively,[48c] we calculated BVS values for the series of complexes listed in Table 4. Good agreement (±0.25) between the BVS and the copper oxidation state is evident for a range of *bona fide* Cu(II) compounds, including those ligated by 1,4,7-triazacyclononanes (entries 1−4) and those containing relatively short copper-oxo or -hydroxo bonds (entries 5−8). In contrast, BVS values significantly greater than 2.0 are obtained when the Cu(II) r_0 values are used for the few crystallographically characterized Cu(III) complexes (entries 9−13) and the bis(μ-oxo)dicopper compounds structurally defined by X-ray crystallography (L = L^{Bn_3}; entry 14) or EXAFS (L = L^{iPr_3}, vide infra; entry 15). Moreover, by using new r_0 values for Cu(III)-N and -O bonds of 1.738 and 1.753, respectively, that were calculated from the data available for the Cu(III) compounds in entries 9, 10, and 12, we obtained BVS = 3.0 ± 0.25 for all the Cu(III) species (entries 9−13) and the bis(μ-oxo)dicopper complexes (entries 14 and 15). Thus, BVS analysis supports assignment of a +3 oxidation state to the copper ions in the bis(μ-oxo) compounds, notwithstanding the approximations inherent to using a small reference database for the derivation of the Cu(III) parameters.

An additional noteworthy feature of the X-ray crystal structure of $[(d_{21}\text{-}L^{Bn_3}Cu)_2(\mu\text{-}O)_2](SbF_6)_2$ is the presence of an array of

(41) Lee, S. C.; Holm, R. H. *J. Am. Chem. Soc.* **1993**, *115*, 11789−11798.

(42) tppa = tris[(6-pivaloylamino)-2-pyridyl)methyl]amine; see ref 4.

(43) L′ = 3-(phenylimimo)butanone 2-oxime; Butcher, R. J.; O'Connor, C. J.; Sinn, E. *Inorg. Chem.* **1981**, *20*, 537−545.

(44) Karlin, K. D.; Nanthakumar, A.; Fox, S.; Murthy, N. N.; Ravi, N.; Huynh, B. H.; Orosz, R. D.; Day, E. P. *J. Am. Chem. Soc.* **1994**, *116*, 4753−4763.

(45) Diaddario, L. L.; Robinson, W. R.; Margerum, D. W. *Inorg. Chem.* **1983**, *22*, 1021−1025.

(46) (a) Clark, G. R.; Skelton, B. W.; Waters, T. N. *J. Chem. Soc., Dalton Trans.* **1976**, 1528−1536. (b) Birker, P. J. M. W. L. *Inorg. Chem.* **1977**, *16*, 2478−2482.

(47) A Cu_2O cluster examined in the gas phase using photoelectron spectroscopy and density functional calculations has been assigned geometric (Cu-O = 1.78 Å) and vibrational (ν_{rhomb} = 630 cm^{-1}) properties similar to those described here: Wang, L.-S.; Wu, H.; Desai, S. R.; Lou, L. *Phys. Rev. B* **1996**, *53*, 8028−8031.

(48) (a) Brown, I. D.; Altermatt, D. *Acta Crystallogr.* **1985**, *B41*, 240−244, 244−247. (b) Thorp, H. H. *Inorg. Chem.* **1992**, *31*, 1585−1588. (c) Hati, S.; Datta, D. *J. Chem. Soc., Dalton Trans.* **1995**, 1177−1182.

Table 4. Bond Valence Sums for Copper Ions in Selected Complexes

entry	compound	coord sphere	Cu−N (Å)	Cu−O (Å)	BVS[a] [Cu(II) r_0]	BVS[b] [Cu(III) r_0]	ref
1	$[(L^{Bn_3}Cu)(L^{Bn_2H}Cu)(\mu\text{-}OH)_2](O_3SCF_3)_2$	3N, 2O	2.054, 2.087, 2.289 2.029, 2.085, 2.266	1.924, 1.949 1.921, 1.940	1.99 2.05		this work (X-ray)
2	$[(L^{iPr_2H}Cu)_2(\mu\text{-}OH)_2](BPh_4)_2$	3N, 2O	2.017, 2.086, 2.303 2.008, 2.048, 2.335	1.922, 1.951 1.930, 1.951	2.02 2.05		this work (X-ray)
3	$[(L^{iPr_2Bn}Cu)_2(\mu\text{-}OH)_2](O_3SCF_3)_2$	3N, 2O	2.113, 2.065, 2.260 2.090, 2.053, 2.266	1.950, 1.933 1.975, 1.967	1.95 1.91		this work (X-ray)
4	$L^{iPr_3}Cu(O_2CCH_3)_2$	3N, 2O	2.132, 2.088, 2.288	1.936, 1.957	1.88		h
5	$[Cu(Me_6tren)(OH)]ClO_4$	4N, O	2.049, 2.189, 2.161, 2.163	1.875	1.88		41
6	$[(OEP)Fe-O-Cu(Me_6tren)]ClO_4$[c]	4N, O	2.045, 2.120, 2.179, 2.157	1.830	2.01		41
7	$[(F_8\text{-}TPP)Fe-O-Cu(TMPA)]ClO_4$[d]	4N, O	2.100, 2.009, 2.172, 1.984	1.856	2.22		44
8	$[L'_3Cu(O)(ClO_4)]_2$[e]	2N, 2O	1.991, 1.98 1.988, 1.971 1.999, 1.980	1.854, 1.956 1.860, 1.958 1.890, 1.999	2.07 2.07 1.95		43
9	$KCuO_2$	4O		1.85, 1.85, 1.85, 1.85	2.59	3.04	21
10	$(Bu_4N)\{Cu[o\text{-}C_6H_4(NCONHCONH)_2]\}$	4N	1.82, 1.85, 1.86, 1.89		2.78	3.04	46b
11	$[Cu(H_{-2}Aib)_3]$[f]	3N, O	1.804, 1.801, 1.898	1.826	2.88	3.21	45
12	$[L^{N_4}Cu(OH)]ClO_4$[g]	4N, O	1.86, 1.87, 1.85, 1.88	2.74	2.63	2.98	46a
13	$SrLaCuO_4$	5O		1.88 (eq), 1.88 (eq), 1.88 (eq), 1.88 (eq), 2.23 (ax)	2.71	2.99	22
14	$[(d_{21}\text{-}L^{Bn_3}Cu)_2(\mu\text{-}O)_2](SbF_6)_2$	3N, 2O	1.986, 1.987, 2.298	1.808, 1.803	2.60	2.96	this work (X-ray)
15	$[(L^{iPr_3}Cu)_2(\mu\text{-}O)_2](ClO_4)_2$	3N, 2O	1.89, 1.89, 2.3 (assumed)	1.89, 1.89	2.60	2.94	this work (EXAFS)

[a] Calculated using r_0 values Cu(II)−O = 1.679 Å and Cu(II)−N = 1.719 Å. Separate BVS values are reported for polynuclear complexes in which the metal ions are inequivalent. [b] Calculated using r_0 values Cu(III)−O = 1.738 Å and Cu(III)−N = 1.753 Å. These parameters, which are necessarily approximate due to the limited available database, were obtained from r_{ij} data for entries 9, 10, and 12. [c] Calculated for one of the independent molecules (no. 2) in the unit cell of the CH_3CN solvate; OEP = octaethylporphyrinate. [d] F_8-TPP = tetrakis(2,6-difluorophenyl)porphyrinate. [e] L′H = 3-(phenylimino)butanone 2-oxime. [f] Aib = tri-α-aminoisobutyric acid. [g] L^{N_4} = planar, tetradentate ligand derived from condensation of oxalyldihydrazide, ammonia, and acetaldehyde. [h] Halfen, J. A.; Tolman, W. B. *J. Am. Chem. Soc.* **1994**, *116*, 5475−5476.

Table 5. Structural Parameters for Selected Complexes with Bis(μ-oxo/hydroxo)dimetal Cores

core structure	supporting ligand[a]	M···M (Å)	O···O (Å)	M−O (Å)	M−O−M (deg)	ref
$Mn^{II,II}_2(\mu\text{-}OH)_2$	Tp^{iPr_2}	3.314(1)	2.553(7)	2.094(4) 2.089(5)	104.8(2)	b
$Mn^{III,III}_2(\mu\text{-}O)_2$	Tp^{iPr_2}	2.696(2)	2.369(8)	1.806(5) 1.813(6) 1.808(6) 1.787(6)	96.5(3) 97.0(3)	b
$Mn^{III,IV}_2(\mu\text{-}O)_2$	phen	2.695(9)	2.425(8)	1.805(5) 1.820(5)	96.0	c
$Mn^{IV,IV}_2(\mu\text{-}O)_2$	phen	2.748(2)	2.326(4)	1.805(3) 1.798(3)	99.5(2)	c
$Fe^{III,III}_2(\mu\text{-}O)_2$	6-Me_3-TPA	2.714(2)		1.841(4) 1.917(4)	92.5(2)	29a
$Fe^{III,III}_2(\mu\text{-}O)(\mu\text{-}OH)$	6-Me_3-TPA	2.95(1)	2.53(1)	1.906(8) 1.981(8)	98.7(4)	d
$Fe^{III,IV}_2(\mu\text{-}O)_2$	5-Me_3-TPA	2.89[e]		1.77[e] 1.94		29b
$Cu^{III,III}_2(\mu\text{-}O)_2$	L^{Bn_3}	2.794(2)	2.287(2)	1.808(5) 1.803(5)	101.4(2)	this work (X-ray)
	L^{iPr_3}	2.88[e]		1.89[e]		this work (EXAFS)
$Cu^{II,II}_2(\mu\text{-}OH)_2$	L^{Bn_3}, L^{Bn_2}	2.9769(9)	2.454(2)	1.949(4) 1.924(5) 1.940(4) 1.921(5)	100.8(2) 100.5(2)	this work
	L^{iPr_2H}	3.0088(13)	2.445(5)	1.922(6) 1.951(6) 1.930(6) 1.951(6)	100.9(3) 102.7(3)	this work
	L^{iPr_2Bn}	3.037(3)	2.42(1)	1.950(6) 1.933(6)	102.9(3)	this work
		3.033(3)	2.49(1)	1.975(6) 1.947(6)	101.3(3)	

[a] Tp^{iPr_2} = hydrotris(3,5-diisopropyl-1-pyrazolyl)borate; phen = 1,10-phenanthroline; 5-Me_3-TPA = tris(5-methylpyridyl-2-methyl)amine. [b] Kitajima, N.; Singh, U. P.; Amagai, H.; Osawa, M.; Moro-oka, Y. *J. Am. Chem. Soc.* **1991**, *112*, 7757−7758. [c] Stebler, M.; Ludi, A.; Bürgi, H.-B. *Inorg. Chem.* **1986**, *25*, 4743−4750. [d] Zang, Y.; Pan, G.; Que, L., Jr.; Fox, B. G.; Münck, E. *J. Am. Chem. Soc.* **1994**, *116*, 3653−3654. [e] From EXAFS.

intramolecular C−D···O hydrogen bonds involving the benzylic C−D bonds and the bridging oxo group (Figure 9). Characterization of C−H···O interactions in organic crystals has been discussed extensively,[49−51] the recent analyses by Steiner and

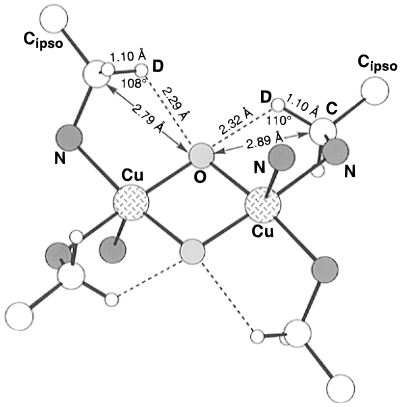

Figure 9. Chem3D representation of the hydrogen bonding interactions in the core of $[(d_{21}\text{-}L^{Bn_3}Cu)_2(\mu\text{-}O)_2](SbF_6)_2$ as determined by X-ray crystallography, but using corrected C−D distances of 1.10 Å that slightly affect other distances and angles involving the D atoms.

Saenger of carbohydrate data on the basis of metrical parameters $d_{H\cdots O}$, $d_{C\cdots O}$, and $\alpha_{CH\cdots O}$ (the C−H−O angle) being particularly pertinent to this discussion.[50,51] In an examination of C−H···O interactions in crystal structures obtained by neutron diffraction, they noted a prominent class of intramolecular hydrogen bonds involving H and O atoms separated by four covalent bonds (formally *S*5,[52] where *S* denotes "self" and 5 refers to the number of atoms in the ring):

Mean geometric parameters for this type of interaction, which do vary over a significant range, are $d_{H\cdots O} = 2.60$ Å, $d_{C\cdots O} = 2.92$ Å, and $\alpha_{CH\cdots O} = 96°$. Comparison of these parameters with those for the bis(μ-oxo)dicopper complex shown in Figure 9 supports the presence of such intramolecular hydrogen bonds in this molecule, as shown by the $d_{H\cdots O}$ (corrected by extending the 0.99 Å C−D distance assigned by X-ray crystallography to 1.10 Å) and the more accurately determined $d_{C\cdots O}$ values in the complex that are shorter than the mean values for the carbohydrates. We also note that the $d_{H\cdots O}$ (either using the X-ray C−H distance of 0.99 Å or the corrected distance of 1.10 Å) are shorter than the sum of the van der Waals radii of the O and H atoms (∼2.7 Å),[53] although it has been argued that the importance of this observation in an analysis of C−H···O hydrogen bonding is questionable.[50] In any case, it is clear that C−H···O bonding interactions exist in the solid state structure of the bis(μ-oxo)dicopper compound. These ground state interactions may be important in the mechanism by which these molecules decompose via oxidative N-dealkylation, which involves rate-determining cleavage of the hydrogen-bonded C−H bonds,[35] as well as in their vibrational spectroscopic properties (see discussion of Raman data below).

X-ray Absorption Spectroscopy. Analysis of EXAFS data collected on solid samples of $[(LCu)_2(\mu\text{-}O)_2](ClO_4)_2$ ($L = L^{Bn_3}$ or L^{iPr_3}) corroborated the X-ray crystallographic results for the complex capped by L^{Bn_3} and allowed definition of the core for the analogous compound ligated by L^{iPr_3}. The r'-space spectra for both complexes (top plots in Figures 10 and 11) are dominated by intense features at $r' \approx 1.5$ Å and $r' \approx 2.5$ Å, corresponding to scatterers in the first and second coordination spheres, respectively, where the copper-scatterer distance r

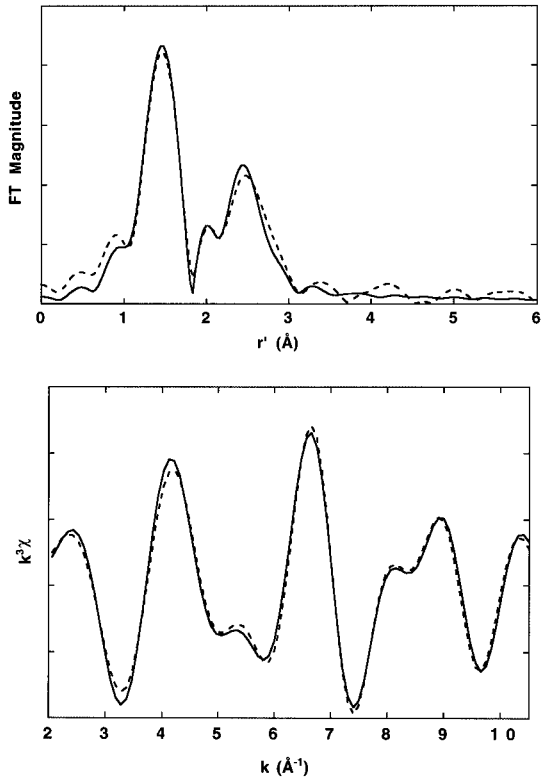

Figure 10. EXAFS data ($k = 2-10.5$ Å^{-1}) (- - -) and simulations (—) for $[(L^{Bn_3}Cu)_2(\mu\text{-}O)_2](ClO_4)_2$: (top) r'-space spectrum; (bottom) k-space spectrum.

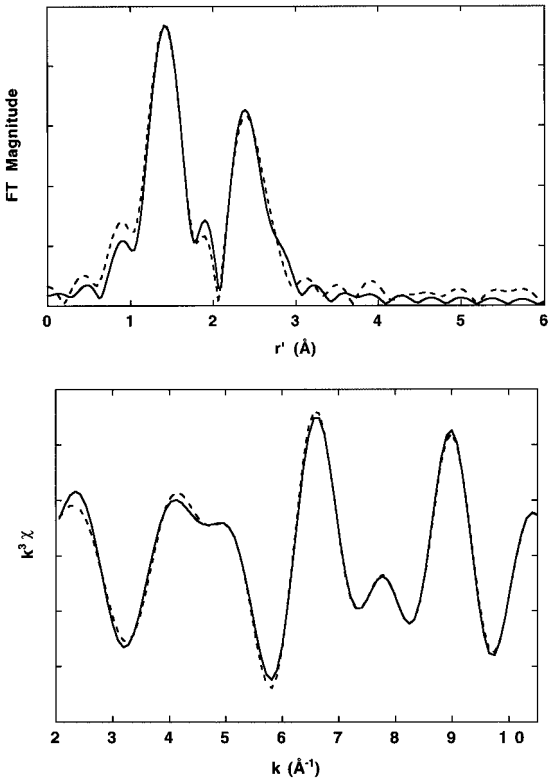

Figure 11. EXAFS data ($k = 2-10.5$ Å^{-1}) (- - -) and simulations (—) for $[(L^{iPr_3}Cu)_2(\mu\text{-}O)_2](ClO_4)_2$: (top) r'-space spectrum; (bottom) k-space spectrum.

(49) For example, see: (a) Green, R. D. *Hydrogen Bonding by C-H Groups*; Wiley: New York, 1974. (b) Taylor, R.; Kennard, O. *J. Am. Chem. Soc.* **1982**, *104*, 5063−5070.

(50) Steiner, T.; Saenger, W. *J. Am. Chem. Soc.* **1992**, *114*, 10146−10154 and references cited therein.

(51) For additional, relevant analyses of C−H···O hydrogen bonds involving (a) water molecules see: Steiner, T.; Saenger, W. *J. Am. Chem. Soc.* **1993**, *115*, 4540−4547, and (b) carbonyl ligands in organometallic complexes see: Braga, D.; Grepioni, F.; Biradha, K.; Pedireddi, V. R.; Desiraju, G. R. *J. Am. Chem. Soc.* **1995**, *117*, 3156−3166.

(52) Etter, M. C.; MacDonald, J. C.; Bernstein, J. *Acta Crystallogr.* **1990**, *B46*, 256−262.

(53) Bondi, A. *J. Phys. Chem.* **1964**, *68*, 441−451.

Table 6. EXAFS Analysis of $[(LCu)_2(\mu\text{-}O)_2](ClO_4)_2$ (L = L^{Bn_3} or L^{iPr_3}) and $[(L^{iPr_3}Cu)_2(\mu\text{-}OH)_2](ClO_4)_2$[9]

	1st sphere		2nd sphere		
	r	σ^2	r	σ^2	ϵ^2 ($\times 10^4$)
$[(L^{Bn_3}Cu)_2(\mu\text{-}O)_2](ClO_4)_2$[a]	4 O/N at 1.90 Å	0.002			30.4
	4 O/N at 1.90 Å	0.002	1 Cu at 2.84 Å	0.005	9.2
	4 O/N at 1.90 Å	0.002	1 Cu at 2.86 Å	0.005	
			9 C at 2.79 Å	0.006	2.0
$[(L^{iPr_3}Cu)_2(\mu\text{-}O)_2](ClO_4)_2$[b]	4 O/N at 1.89 Å	−0.001			34.0
	4 O/N at 1.89 Å	0.000	1 Cu at 2.88 Å	0.003	8.7
	4 O/N at 1.89 Å	0.000	1 Cu at 2.86 Å	0.005	
			9 C at 2.94 Å	0.004	1.3
$[(L^{iPr_3}Cu)_2(\mu\text{-}OH)_2](ClO_4)_2$[c]	4 O/N at 1.99 Å	0.005			
	1 N at 2.30 Å	0.004			14.4
	4 O/N at 1.98 Å	0.005			
	1 N at 2.29 Å	0.004	1 Cu at 3.07 Å	0.009	12.2
	4 O/N at 1.98 Å	0.005	1 Cu at 3.08 Å	0.006	
	1 N at 2.30 Å	0.006	7 C at 2.91 Å	0.005	6.0

[a] Fourier transform range 2−10.5 $Å^{-1}$, back-transform range 1−3.1 Å. [b] Fourier transform range 2−10.5 $Å^{-1}$, back-transform range 1−3.0 Å. [c] Fourier transform range 2−14.0 $Å^{-1}$, back-transform range 1−3.3 Å.

approximately equals $r' + 0.4$ Å. In terms of overall appearance, the spectra closely resemble those reported previously for complexes or proteins with bis(μ-oxo)diiron[29] and -dimanganese cores.[30,54] In these iron and manganese EXAFS r'-space spectra, the prominent second-sphere feature is attributed to a metal ion scatterer at ∼2.7−3.0 Å. Similarly, we assign the second-sphere features in the EXAFS spectra for the bis(μ-oxo)dicopper complexes to a Cu scatterer, with additional contributions from C atoms in the ligand backbone.

The best fits to the *k*-space spectra are summarized in Table 6 and shown in Figures 10 and 11. In both cases, the first coordination sphere feature was best fit using a single shell of four O/N scatterers at 1.89−1.90 Å, which corresponds to the average of the Cu−μ-O (1.81 Å) and Cu−N_{eq} (1.99 Å) bond lengths found in the crystal structure of $[(d_{21}\text{-}L^{Bn_3}Cu)_2(\mu\text{-}O)_2](SbF_6)_2$. Splitting of this shell into two subshells was not possible due to the limited resolution of the data sets (k = 2−10.5 $Å^{-1}$, Δr = 0.19 Å).[55] The ∼2.3 Å Cu−N_{ax} distance observed in the crystal structure was not required to obtain a good fit.

The second coordination sphere was best fit with a copper scatterer at 2.86 Å and additional carbon scatterers in both of the L^{Bn_3}- and L^{iPr_3}-capped complexes. Attempted fits using only Cu or only C to model the second-sphere feature were of poorer quality. However, the Cu···Cu distances determined by analysis of the EXAFS data were 0.07 Å longer than that determined by X-ray crystallography {Cu···Cu = 2.79 Å in $[(d_{21}\text{-}L^{Bn_3}Cu)_2(\mu\text{-}O)_2](SbF_6)_2$}. A similar ∼0.07 Å shift in the Cu···Cu distance was observed in the EXAFS analysis of $[(L^{iPr_3}Cu)_2(\mu\text{-}OH)_2](ClO_4)_2$ compared to the crystal structure of its L^{iPr_2H}-capped analog. We attribute this apparently systematic discrepancy to the Cu-shell parameters used in the EXAFS analysis, which were derived from data acquired for $[Cu(TMEN)(\mu\text{-}OH)]_2Br_2\cdot H_2O$ (TMEN = tetramethylethylenediamine).[56] There are a number of carbon atoms at similar distance as the other copper atom in this structure, and the resulting interference between the Cu and C atoms makes it somewhat difficult to extract accurate parameters for the Cu-only or C-only shells. In any case, the correspondence between the EXAFS data and fits for the bis(μ-oxo)dicopper complexes ligated by L^{Bn_3} or L^{iPr_3}, in conjunction with the general agreement of the former with the X-ray crystallographic data, indicates that the $[Cu_2(\mu\text{-}O)_2]^{2+}$ core structure is basically the same for both compounds.

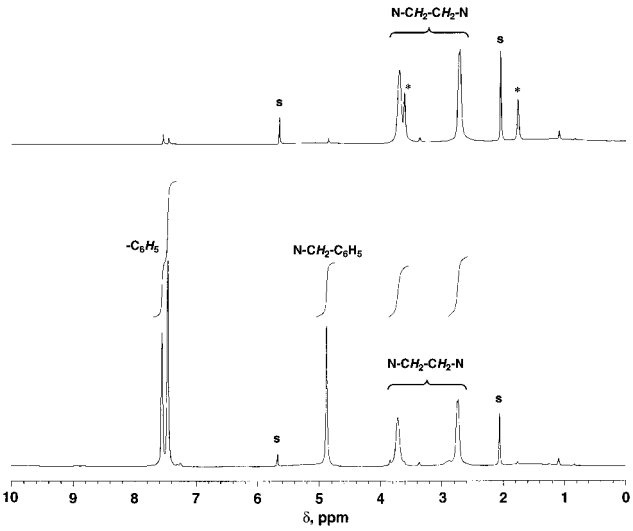

Figure 12. 500 MHz ^1H NMR spectra of (top) $[(d_{21}\text{-}L^{Bn_3}Cu)_2(\mu\text{-}O)_2](ClO_4)_2$ and (bottom) $[(L^{Bn_3}Cu)_2(\mu\text{-}O)_2](ClO_4)_2$ in 2:1 $(CD_3)_2CO/CD_2Cl_2$ at −75 °C (s denotes peaks due to residual hydrogen atoms in the solvents; * indicates THF impurity present in the Cu(I) precursor).

NMR Spectroscopy. In Figure 12 are shown ^1H NMR spectra for $[(L^{Bn_3}Cu)_2(\mu\text{-}O)_2](ClO_4)_2$ (bottom) and $[(d_{21}\text{-}L^{Bn_3}Cu)_2(\mu\text{-}O)_2](ClO_4)_2$ (top) in 2:1 $(CD_3)_2CO/CD_2Cl_2$ at −75 °C. Comparison of the two spectra allows assignment of the peaks as shown. The chemical shifts differ from those of the Cu(I) starting materials {7.3, 3.9, 2.7, 2.5, and 2.4 ppm for $[L^{Bn_3}Cu(CH_3CN)]ClO_4$ at −75 °C}, which are clearly not present in these solutions, but the differences are not as large as would be expected if there were significant paramagnetic contributions. Thus, the presence of sharp peaks with chemical shifts in the 0−10 ppm region and the absence of signals in EPR spectra clearly indicate that the bis(μ-oxo)dicopper compounds are diamagnetic. Sharp resonances in the normal regions also are present in $^{13}C\{^1H\}$ NMR spectra (Table 1). The simplicity of the NMR spectra is not consistent with the structure of the complex as determined in the solid state, which would be expected to have many more inequivalent hydrogens due to the asymmetry inherent to the square pyramidal copper coordination

(54) Recent lead references: (a) DeRose, V. J.; Mukerji, I.; Latimer, M. J.; Yachandra, V. K.; Sauer, K.; Klein, M. P. *J. Am. Chem. Soc*. **1994**, *116*, 5239−5249. (b) Riggs-Gelasco, P. J.; Mei, R.; Yocum, C. F.; Penner-Hahn, J. E. *J. Am. Chem. Soc*. **1996**, *118*, 2387−2399.

(55) The data collected for both complexes contained significant artifacts in the region above k = 10.5 $Å^{-1}$ which could not be corrected for. These artifacts may have arisen from imperfections in the monochromator crystal used in the data collection. The use of data beyond k = 10.5 $Å^{-1}$ (as was reported previously)[27] engendered artifactual features in their Fourier-transformed spectra that could only be fit with parameters requiring unreasonably negative $\Delta\sigma^2$ values.

(56) Mitchell, T. P.; Bernard, W. H.; Wasson, J. R. *Acta Crystallogr*. **1970**, *B26*, 2096.

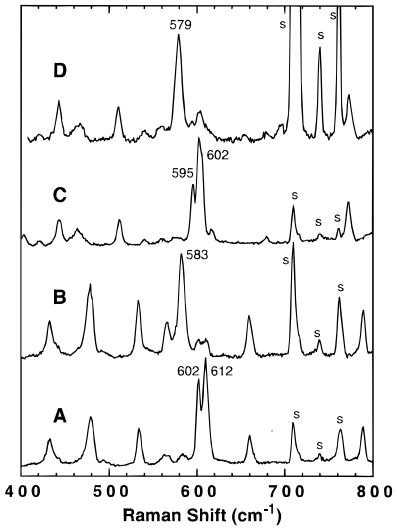

Figure 13. Resonance Raman spectra obtained with 457 nm excitation on frozen (77 K) CH_2Cl_2 solutions of (A) $[(L^{Bn_3}Cu)_2(\mu\text{-}O)_2](ClO_4)_2$, (B) $[(L^{Bn_3}Cu)_2(\mu\text{-}^{18}O)_2](ClO_4)_2$, (C) $[(d_{21}\text{-}L^{Bn_3}Cu)_2(\mu\text{-}O)_2](ClO_4)_2$, and (D) $[(d_{21}\text{-}L^{Bn_3}Cu)_2(\mu\text{-}^{18}O)_2](ClO_4)_2$. Peaks most sensitive to oxygen isotope substitution are labeled with their Raman shifts; s denotes bands derived from CH_2Cl_2 solvent.

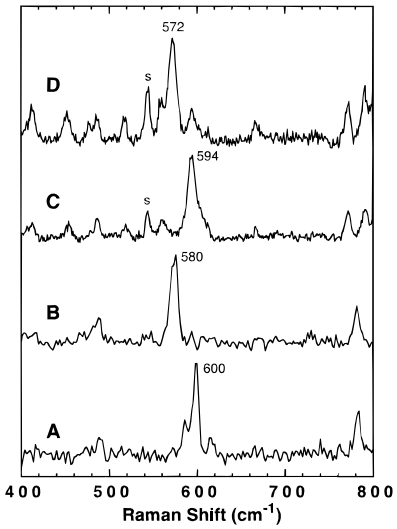

Figure 14. Resonance Raman spectra obtained with 457 nm excitation on frozen (77 K) solutions of (A) $[(L^{iPr_3}Cu)_2(\mu\text{-}O)_2](ClO_4)_2$ in THF, (B) $[(L^{iPr_3}Cu)_2(\mu\text{-}^{18}O)_2](ClO_4)_2$ in THF, (C) $[(L^{iPr_2Bn}Cu)_2(\mu\text{-}O)_2](ClO_4)_2$ in acetone, and (D) $[(L^{iPr_2Bn}Cu)_2(\mu\text{-}^{18}O)_2](ClO_4)_2$ in acetone. Peaks most sensitive to oxygen isotope substitution are labeled with their Raman shifts; s denotes bands derived from acetone solvent; peaks due to THF solvent in spectra A and B have been removed by subtraction.

environments. A rapid fluxional process must occur in solution to interchange the inequivalent equatorial and axial coordination positions and thus simplify the spectra, but the nature of this process(es) is not known. We favor an intramolecular rearrangement (cf. turnstile rotation), primarily in view of the results of cross-over experiments presented elsewhere[35] that argue against the generation of monomeric fragments or the interchange of capping triazacyclononane ligands in solutions of the bis(μ-oxo)dicopper compounds. Theoretical calculations also support a low energy barrier for an intramolecular half-turnstile rotation process (vide infra).

Resonance Raman Spectroscopy. Further structural insights into the unique bis(μ-oxo)dicopper cores were obtained from analysis of resonance Raman spectra collected on frozen solutions at 77 K using 457.9 nm excitation (nearly coincident with the longer wavelength CT absorption band of the complexes). Spectra of solutions of $[(L^{Bn_3}Cu)_2(\mu\text{-}O)_2](ClO_4)_2$ and isotopomers with perdeuterated benzyl substituents and/or ^{18}O in the core in CH_2Cl_2 are shown in Figure 13. Data for ^{16}O- and ^{18}O-substituted complexes capped by L^{iPr_3} (in THF) and L^{iPr_2Bn} (in acetone) are presented in Figure 14, with oxygen isotope-sensitive features for all spectra listed in Table 1.

While a number of resonance enhanced Raman features are evident in the spectra, only one set of features near $\sim$600 cm^{-1} is common to all of the complexes and is sensitive to ^{18}O-substitution. For L = L^{iPr_3}, a prominent peak is observed at 600 cm^{-1} which shifts to 580 cm^{-1} upon ^{18}O substitution; the corresponding features for L^{iPr_2Bn} are found at 594 and 572 cm^{-1}, respectively. Interestingly for L = L^{Bn_3}, there are two peaks at 602 and 612 cm^{-1}, which shift to 583 cm^{-1} when the complex is prepared with $^{18}O_2$. The conversion of the two features in the complex generated with $^{16}O_2$ to one when the complex is generated with $^{18}O_2$ suggests that the doublet results from a Fermi resonance of the oxygen-sensitive vibration and an overtone of a fundamental vibration near 300 cm^{-1} or a combination band arising from the ligand. Similar behavior has been noted for $[Fe_2O_2(5\text{-}Me_3\text{-}TPA)_2]^{3+}$ [5-Me$_3$-TPA = tris-(5-methylpyridyl-2-methyl)amine].[29b] We assign these ^{18}O-sensitive features at $\sim$600 cm^{-1} to an A_1 vibration of the $[Cu_2(\mu\text{-}O)_2]^{2+}$ core, by analogy to those of related $[M_2(\mu\text{-}O)_2]^{3+}$ units (M = Fe or Mn) at 660−700 cm^{-1}.[29,57] The slightly higher energies of the latter features are likely due to a combination of factors, including higher charge and smaller masses of the metal centers and variations in the M−O−M angles. In support of the vibrational assignment, the ^{18}O isotope shifts for all of the copper complexes are 20−24 cm^{-1}, approaching the expected shift of 28 cm^{-1} for a simple Cu−O harmonic oscillator at 600 cm^{-1}. As described below, the observed frequency and isotope shift agree well with those of the theoretically calculated $[Cu_2(\mu\text{-}O)_2]^{2+}$ rhomb [$\nu(^{16}O)$ = 630 cm^{-1}; $\Delta(^{18}O)$ = 29 cm^{-1}].[47] Finally, the ca. 600 cm^{-1} feature for $[(d_{21}\text{-}L^{Bn_3}Cu)_2(\mu\text{-}O)_2](ClO_4)_2$ exhibits a depolarization ratio of 0.57 in CH_2Cl_2 at −80 °C, signifying that the core vibration is polarized and totally symmetric,[58] consistent with our A_1 assignment.

We have also observed that the $Cu_2(\mu\text{-}O)_2$ core vibration is sensitive to substitution of deuterium into the benzyl substituents of L^{Bn_3}, downshifting by 7−10 cm^{-1} for the ^{16}O compound and 4 cm^{-1} for the ^{18}O analog; this effect is much less pronounced for L = L^{iPr_3}. This intriguing effect of benzylic deuteration indicates coupling of ligand-based vibrations with that of the $Cu_2(\mu\text{-}O)_2$ core. The coupling may be rationalized by consideration of the X-ray crystal structure of $[(d_{21}\text{-}L^{Bn_3}Cu)_2(\mu\text{-}O)_2](SbF_6)_2$ which shows the presence of interactions between the oxo bridges and the benzylic deuterium atoms (vide supra); these interactions may provide the conduit for the vibrational coupling. Following this reasoning, the absence of a significant effect of deuteration on the 600 cm^{-1} feature of the L^{iPr_3} complexes suggests that such C−H···O interactions may be less important in the latter compounds, a hypothesis that needs corroboration. Whatever the rationale for the deuterium effect, the near constancy of the 600 cm^{-1} vibration across the variety of triazacyclononane ligands studied argues that the assignment of this mode to a $Cu_2(\mu\text{-}O)_2$ core remains a good approximation.

(57) (a) Czernuszewicz, R. S.; Dave, B.; Rankin, J. G. In *Spectroscopy of Biological Molecules*; Hester, R. E., Girling, R. B., Eds.; Royal Society of Chemistry: Cambridge, 1991; pp 285−288. (b) Gamelin, D. R.; Kirk, M. L.; Stemmler, T. L.; Pal, S.; Armstrong, W. H.; Penner-Hahn, J. E.; Solomon, E. I. *J. Am. Chem. Soc.* **1994**, *116*, 2392−2399.

(58) Nakamoto, K. *Infrared and Raman Spectra of Inorganic and Coordination Compounds*, 4th ed.; John Wiley & Sons: New York, 1986; pp 72−76.

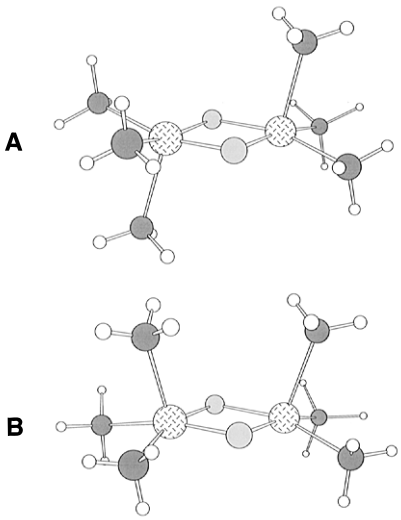

Figure 15. Structures for anti (A) and eclipsed (B) $\{[(NH_3)_3Cu]_2(\mu\text{-}O)_2\}^{2+}$ (optimized at the RHF/STO-3G level).

Table 7. Selected Bond Lengths (Å) and Angles (deg) for Calculated and Experimental $[Cu_2(\mu\text{-}O)_2]^{2+}$ Complexes

	anti $\{[(NH_3)_3Cu]_2(\mu\text{-}O)_2\}^{2+}$	eclipsed $\{[(NH_3)_3Cu]_2(\mu\text{-}O)_2\}^{2+}$	$[(d_{21}\text{-}L^{Bn_3}Cu)_2(\mu\text{-}O)_2](SbF_6)_2$
Cu−Cu	2.734	2.741	2.794
O−O	2.281	2.275	2.287
Cu−O	1.780	1.781	1.803, 1.808
$Cu-N_{axial}$	2.207	2.205	2.298
$Cu-N_{equatorial}$	1.996	2.000	1.986, 1.987
O−Cu−O	79.7	79.4	78.6
Cu−O−Cu	100.3	100.6	101.4
$O-Cu-N_{axial}$	100.9	103.9	102.3, 103.8
$O-Cu-N_{eq,syn}$	90.7	90.0	95.6, 96.2
$O-Cu-N_{eq,anti}$	163.7	161.5	171.1, 172.3

Nevertheless, it is clear that the Raman spectra of these $Cu_2(\mu\text{-}O)_2$ complexes provide a wealth of information that has yet to be mined. For the L^{iPr_3} case, low intensity peaks at 614 and 588 cm^{-1} that are sensitive to both ^{18}O and deuterium substitution have yet to be assigned. The remaining, non-^{18}O-sensitive peaks in the spectra of all the compounds shift upon ligand deuteration to varying extents and are therefore attibutable to ligand-based vibrations with at least partial substituent $C-CH_n$ stretching and/or bending character. A detailed Raman study of these features is in progress and will be the subject of a future report.[59]

Theoretical Calculations. In order to obtain insights into the stability and electronic structure of the novel bis(μ-oxo)-dicopper core *ab initio* calculations at the restricted Hartree Fock (RHF) level using the STO-3G basis set were performed on the model system $\{[(NH_3)_3Cu]_2(\mu\text{-}O)_2\}^{2+}$; the experimental X-ray crystallographic coordinates for corresponding atoms in $[(d_{21}\text{-}L^{Bn_3}Cu)_2(\mu\text{-}O)_2](SbF_6)_2$ were used as a starting point. Two different local minima, both of which are closed-shell singlet states, were found for $\{[(NH_3)_3Cu]_2(\mu\text{-}O)_2\}^{2+}$ at the RHF/STO-3G level of theory; they are illustrated in Figure 15. The major difference between the structures is the relative disposition of the axial N-donor ligands, anti in structure A versus eclipsed in structure B. The critical heavy atom−heavy atom bond lengths and angles in these structures are provided in Table 7, together with those determined from the X-ray crystal structure of $[(d_{21}\text{-}L^{Bn_3}Cu)_2(\mu\text{-}O)_2](SbF_6)_2$, which has an anti arrangement of axial N-ligands. Overall, the agreement between the theoretical and experimental anti structures is remarkable. The largest deviations are observed for the various bond angles O−Cu−N, but this is only to be expected insofar as the ammonia nitrogen atoms in the theoretical structure are unconstrained in contrast to those found in the triazacyclononane ligands. In addition, the Cu−O bonds are too short in the theoretical structure by about 0.025 Å. This may be attributable to the electronic and steric differences between the ammonia ligands and the triazacyclononanes and/or it may reflect the overbinding associated with the single-determinant RHF wave function (vide infra). In any case, it appears possible that this level of theory will continue to be useful for providing reasonably accurate structures for future modeling studies.

Table 8. Relative Energies (kcal/mol) of $\{[(NH_3)_3Cu]_2(\mu\text{-}O)_2\}^{2+}$ Structures[a]

level of theory	anti[b]	eclipsed	TS‡
RHF/STO-3G	0.0	1.8	2.7
Xα/STO-3G	0.0	2.9	2.4
BLYP/STO-3G	0.0	2.3	1.9
CAS(2,2)/DZP	0.0	−1.7	
CASPT2N(2,2)/DZP	0.0	8.7	

[a] All results are at the RHF/STO-3G* geometries. [b] Absolute energies (au) for this column are −3723.975 99, −3718.784 80, −3729.233 71, −3763.304 06, and −3765.175 94.

The relative energies for the two local minima were determined at several different levels of theory, and the results are provided in Table 8. At the RHF/STO-3G level, the two stereoisomers differ by only 1.8 kcal/mol. However, this level of theory should not, *a priori*, be expected to be especially accurate. In addition to the small basis set, the use of a single determinant (implicit in HF theory) may be an inadequate approximation for this system. Simple $[Cu_2(\mu\text{-}\eta^2\text{:}\eta^2\text{-}O_2)]^{2+}$, for instance, has been shown to be characterized by a significant mixing of multiple determinants in its lowest closed-shell singlet state.[60,61] One approach to treat this configurational mixing is to use density functional theory, where the theoretical method optimizes the energy with respect to the total electron density as opposed to the wave function. DFT has been shown for a variety of systems to accurately account for configurational mixing in closed-shell singlets (based on calculations of geometries, multiplet splittings, etc.).[62] Interestingly, the energy difference between the anti and eclipsed conformers increases only slightly when either Xα or the gradient-corrected BLYP levels of density functional theory are employed in place of Hartree−Fock theory. Furthermore, there is no tendency for the α and β Kohn−Sham molecular orbitals to break symmetry. Indeed, symmetry broken starting densities smoothly converge to fully symmetric solutions indistinguishable from restricted calculations. This is in contrast to results obtained for $[Cu_2(\mu\text{-}\eta^2\text{:}\eta^2\text{-}O_2)]^{2+}$ model systems,[63] and may be taken as evidence of the highly covalent nature of the bonding in the $\{[(NH_3)_3Cu]_2(\mu\text{-}O)_2\}^{2+}$ system.[64]

As a more rigorous test of the importance of multiple configurations, we carried out 2-electron-in-2-orbital (2,2) complete active space multiconfiguration self-consistent field calculations (CAS). This calculation permits partial occupation

(59) Wilkinson, E. C.; Rodgers, K.; Mahapatra, S.; Que, L., Jr.; Tolman, W. B. Work in progress.

(60) Maddaluno, J.; Geissner-Prettre, C. *Inorg. Chem.* **1991**, *30*, 3439.

(61) Bernardi, F.; Bottoni, A.; Casadio, R.; Fariselli, P.; Rigo, A. *Int. J. Quantum Chem.* **1996**, *58*, 109−119.

(62) (a) Cramer, C. J.; Dulles, F. J.; Storer, J. W.; Worthington, S. E. *Chem. Phys. Lett.* **1994**, *218*, 387. (b) Cramer, C. J.; Dulles, F. J.; Falvey, D. E. *J. Am. Chem. Soc.* **1994**, *116*, 9787. (c) Cramer, C. J.; Worthington, S. E. *J. Phys. Chem.* **1995**, *99*, 1462. (d) Lim, M. H.; Worthington, S. E.; Dulles, F. J.; Cramer, C. J. In *Density-Functional Methods in Chemistry*; Laird, B. B., Ross, R., Ziegler, T., Eds.; American Chemical Society: Washington, DC, 1996; p 402.

(63) Ross, P. K.; Solomon, E. I. *J. Am. Chem. Soc.* **1991**, *113*, 3246−3259.

(64) Lovell, T.; McGrady, J. E.; Stranger, R.; Macgregor, S. A. *Inorg. Chem.* **1996**, *35*, 3079−3080.

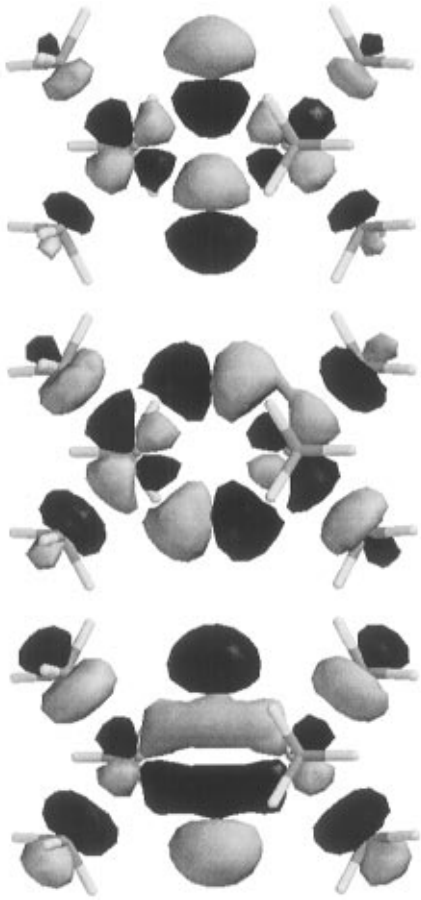

Figure 16. From bottom to top, the HOMO, LUMO, and LUMO + 1 orbitals of anti $\{[(NH_3)_3Cu]_2(\mu\text{-}O)_2\}^{2+}$ calculated at the RHF/STO-3G* level. The plots are for the 0.032 bohr^{-3} isodensity surface.

of both the highest occupied and lowest unoccupied molecular orbitals (HOMO and LUMO, respectively). For the anti isomer, these orbitals are illustrated in Figure 16, along with the LUMO + 1 which will be discussed further below. The HOMO, $12a_u$, is formed from a combination of copper $d_{x^2-y^2}$ orbitals and oxygen p orbitals. The mixing is net bonding between copper and oxygen and copper and copper, but net antibonding between oxygen and oxygen (i.e., it may be thought of as a bonding combination of a copper−copper π bond with an oxygen−oxygen σ* bond). Note that this HOMO is spatially similar to that previously reported for the (μ-η^2:η^2-peroxo)dicopper core,[63] but with greater overlap between the fragment orbitals due to the different interatomic distances in the bis(μ-oxo) unit. The LUMO, $12b_g$, hybridizes copper $d_{x^2-y^2}$ orbitals with oxygen p orbitals in a different manner that is net antibonding between all atoms in the rhomb. This pair of MOs correlates with the HOMO ($13b_1$) and LUMO ($10a_2$) in the eclipsed conformer.

To increase the accuracy of these calculations, a considerably more flexible polarized double-ζ basis set[65] was employed. Although the CAS(2,2) calculations reverse the relative energies of the two conformers, the net effect is only 3.5 kcal/mol. When additional account of correlation is taken via multireference second-order perturbation theory (CASPT2N), the anti isomer is again found to be lower, and moreover by a larger margin, namely 8.7 kcal/mol. From examination of the coefficients associated with the two possible closed-shell singlet determinants (i.e., for the anti conformer $|...12a_u^2 12b_g^0\rangle$ vs $|...12a_u^0 12b_g^2\rangle$), it is apparent that multiconfigurational wave functions are a hallmark of the $\{[(NH_3)_3Cu]_2(\mu\text{-}O)_2\}^{2+}$ system, analogous to the (μ-η^2:η^2-peroxo)dicopper core. In each

(65) Schafer, A.; Horn, H.; Ahlrichs, R. *J. Chem. Phys.* **1992**, *97*, 2571.

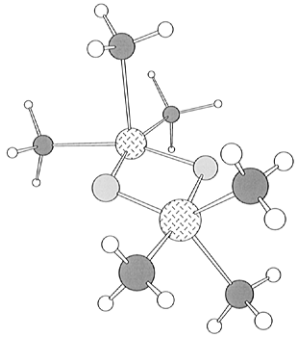

Figure 17. Transition state structure that interconverts anti and eclipsed $\{[(NH_3)_3Cu]_2(\mu\text{-}O)_2\}^{2+}$ (optimized at the RHF/STO-3G* level).

conformer there is a 65:35 mixing of the HOMO^2 and LUMO^2 states. Moreover, the nontrivial difference between the CAS(2,2) and CASPT2N(2,2) relative energies suggests that a larger active space might be important to account for additional important nondynamic correlation effects. However, insofar as we are using these calculations simply to provide some insight into the experimentally characterized systems, we did not examine in detail any more costly calculations employing larger active spaces here.

One noteworthy feature of the CAS calculations is that at this level of theory both the anti and eclipsed conformers are unstable to dissociation into fragments. This can be understood in terms of the substantial contribution of the LUMO^2 configuration, which is antibonding between all rhomb atoms. This feature, combined with the Coulomb repulsion between the two cationic centers, renders the complexes unstable. It is possible that this is an artifact that would disappear were geometry optimization to proceed with further consideration of electron correlation (although we did not find expansion of the active space to (8,8) to be helpful), or it may be that $\{[(NH_3)_3Cu]_2(\mu\text{-}O)_2\}^{2+}$ is indeed unstable to dissociation in the gas phase. Of course, larger ligands, condensed-phase effects, and the presence of counterions, all of which occur for the experimentally characterized systems, would be expected to strongly mitigate the Coulomb repulsion in the dication. In any case, it appears that the RHF/STO-3G level serendipitously provides qualitatively useful geometries and energies through cancelling errors in the various theoretical approximations.

Other results from the theoretical calculations may be used to further our understanding of the experimental behavior of these systems. The observation of stable closed-shell singlet states for the calculated structures corroborates the experimental finding that the bis(μ-oxo) complexes are diamagnetic, as revealed by EPR silence and sharp peaks in the diamagnetic regions of NMR spectra. Moreover, the NMR results imply a low barrier to the exchange of axial and equatorial N-donor ligand positions (note that double-label experiments preclude dissociation/reassociation as the operative mechanism). The small calculated difference in energies for the anti and eclipsed conformers at all levels of theory offers some support for this hypothesis, and to further examine it we located a transition-state structure that interconverts the two conformers via a half-turnstile-like[66] rotation of the nitrogen ligands at one copper atom (Figure 17). The barrier associated with this rotation is only 2.7 kcal/mol at the RHF/STO-3G level. At the density functional levels, the transition state structure is calculated to have a slightly lower energy than the eclipsed structure. Presumably this is simply an artifact of not reoptimizing all of the geometries at this level; the important conclusion to be drawn from these calculations is that the barrier to ligand rotation is

(66) Ugi, I.; Marquarding, D.; Klusacek, H.; Gillespie, P.; Ramirez, F. *Acc. Chem. Res.* **1971**, *4*, 288.

very small. Although this barrier would certainly be expected to increase in the actual experimental systems because of steric congestion present in the eclipsed structures, it still appears quite reasonable to postulate rapid rotation on the NMR time scale at the experimental temperatures.

The verification of the anti and eclipsed structures as local minima at the RHF/STO-3G level was accomplished by analytic frequency calculations. These calculations were then used to determine the frequency shift associated with ^{18}O isotopic substitution for the Raman active rhomb breathing mode discussed above. For the anti conformer, we calculate $\nu(^{16}O) = 633\ cm^{-1}$ and $\nu(^{18}O) = 604\ cm^{-1}$, i.e., a frequency shift of $29\ cm^{-1}$. These data compare favorably with the experimentally observed absorptions and isotopic shifts in the complexes described above and further support the experimental assignments of this fundamental. For the eclipsed conformer, we calculate $\nu(^{16}O) = 630\ cm^{-1}$ and $\nu(^{18}O) = 601\ cm^{-1}$. Although it is possible that the experimental observation of two peaks in the Raman spectrum for this fundamental corresponds to the presence of both anti and eclipsed triazacyclononane conformers (with an accidental isochronicity in the ^{18}O case), this is probably less likely than the above proposed Fermi resonance for the ^{16}O case. The steric demands of the triazacyclononane ligands are considerably larger than those of the theoretical ammonia ligands, so that the equilibrium population of the eclipsed conformer might be expected to be below detection limits. In the solid state, on the other hand, it may be that crystal packing effects (involving additionally counterions and solvent molecules) can counter the higher steric energy associated with the eclipsed conformation, and it is intriguing to speculate that this mode of complexation may be observable under suitable conditions and/or in different synthetic or biological systems.

The LUMO + 1 orbital (Figure 16) provides some insight into the apparent electrophilic character exhibited by the rhomb oxygen atoms (as judged by their proclivity to indulge in hydrogen atom abstractions, which is discussed more fully in a separate paper).[35] This $13a_u$ orbital is formed from an all antibonding combination of copper $d_{x^2-y^2}$ orbitals and oxygen p orbitals, i.e., the same fragment orbitals used to construct the $12a_u$ HOMO but taken with opposite phase. In the $12a_u$ HOMO, the copper d orbital coefficients are larger than the oxygen p orbital coefficients; in the $13a_u$ LUMO + 1, it is the oxygen p orbital coefficients that dominate. This orbital would be expected to be quite high in energy in a peroxo species, since it is dominated by σ^*_{OO} character, but the large separation between the oxygen atoms in the rhomb for the bis-oxo motif stabilizes this virtual orbital so that it is only very slightly higher in energy than the $12b_g$ LUMO. The $13a_u$ orbital, a low-energy acceptor orbital dominated by contributions from in-plane oxygen p fragments, thus rationalizes the observed electrophilicity of the rhomb oxygen atoms in the experimental systems.

Finally, a comparison of the HOMO in the bis(μ-oxo) core to that reported for the analogous μ-η^2:η^2-peroxo system[2,63] provides some insight into the formal oxidation levels of the atoms in the core. Because of the large distance between the oxygen atoms in the $[Cu_2(\mu\text{-}O)_2]^{2+}$ rhomb, there is much less energetic cost associated with mixing a substantial fraction of oxygen σ^* into the HOMO than in the peroxo case where the O−O bond is present (and, as noted above, this mixing increases bonding with the copper fragments in the bis(μ-oxo) core). Such hybridization moves electronic charge off of the copper atoms and onto the oxygen atoms relative to the peroxo system. Since the latter are well described as Cu^{II} species, this orbital modification may be used to suggest a formal $[Cu^{III}_2(\mu\text{-}O^{2-})_2]^{2+}$ oxidation state for the bis(μ-oxo)dicopper unit.

Summary and Perspectives

We have constructed a coherent picture of the structure and bonding of a series of bis(μ-oxo)dicopper complexes, which represent a new motif in copper−dioxygen chemistry, through a combination of experimental and theoretical investigations. A topology for the $[Cu_2(\mu\text{-}O)_2]^{2+}$ rhomb characterized by short Cu−O (∼1.80 Å) and Cu···Cu (∼2.80 Å) distances was revealed by X-ray crystallography, EXAFS spectroscopy, and *ab initio* calculations. These interatomic distances are similar to those previously identified in analogous cores comprised of iron or manganese ions and are notably shorter than those typical for bis(μ-hydroxo)dicopper(II) compounds (∼1.95 and ∼3.00 Å, respectively). Examples of the latter type of compound are produced upon decomposition of the thermally unstable bis(μ-oxo)dicopper complexes in reactions involving N-dealkylation of the triazacyclononane ligands, as verified by X-ray crystallographic studies. Spectroscopic and electrospray mass spectrometry experiments showed that the bis(μ-oxo)dicopper core remains intact in solution at low temperature and revealed specific geometric and electronic structural features. For example, we identified a vibrational signature of the $[Cu_2(\mu\text{-}O)_2]^{2+}$ core that is coupled to macrocycle ligand vibrations in resonance Raman spectra of isotopically labeled compounds. In addition, the diamagnetism of the bis(μ-oxo)dicopper species, as well as the existence of a fluxional process in solution that interchanges equatorial and axial N-donor ligand positions, was revealed by low-temperature NMR and EPR spectroscopy. *Ab initio* theory for a model system predicts a closed-shell singlet ground-state structure that agrees well with the experimentally determined geometry and provides a basis for understanding key properties of the bis(μ-oxo)dicopper core, such as its diamagnetism, its resonance Raman signature, and the low barrier to the fluxionality involving the N-donors. These theoretical calculations, in conjunction with analysis of the experimental data, are consistent with a formal portrayal of the core as $[Cu^{III}_2(\mu\text{-}O^{2-})_2]^{2+}$, but further suggest that a molecular orbital description involving a high degree of mixing of oxygen and copper fragment orbitals (i.e. covalency) is appropriate.

The reaction of the LCu(I) precursors with O_2 in a 2:1 ratio to generate bis(μ-oxo)dicopper(III) species stands in stark contrast to the usual process involving a 4:1 stoichiometry and production of μ-oxo- or μ-hydroxo-bridged Cu(II) compounds (eq 1). As in the typical 4:1 reaction, a (μ-peroxo)dicopper(II) complex is a likely intermediate along the pathway to the bis(μ-oxo)dicopper(III) product. Instead of being reduced by additional Cu(I) ions, however, O−O bond cleavage occurs entirely intramolecularly; indeed, we have observed this conversion and its reverse directly for the case where $L = L^{iPr_3}$.[28] In a formal sense, the bis(μ-oxo)dicopper(III) core can be viewed as being derived from homolysis of the (μ-peroxo) O−O bond concomitant with one electron oxidation of each of the copper(II) ions.[67] Thus, the (μ-peroxo)dicopper(II) and bis(μ-oxo)dicopper(III) cores are isomers residing at the same overall oxidation level and, therefore, each can be considered equally competent as potential oxidants in copper/dioxygen chemistry and biochemistry.

The $[Cu_2(\mu\text{-}O)_2]^{2+}$ core also may be envisioned to be a close counterpart of the $[M^{IV}_2(\mu\text{-}O^{2-})_2]^{4+}$ (M = Fe or Mn) unit, which for M = Mn has been structurally defined but which for M = Fe has yet to be identified in a synthetic complex, notwithstanding the fact that it has captured the imagination of those investigating how the diiron active site of methane monooxy-

(67) Detailed theoretical and experimental studies of the actual peroxo/bis(μ-oxo) isomerization process are in progress. See: Cramer, C. J.; Smith, B. A.; Tolman, W. B. *J. Am. Chem. Soc.*, in press.

genase may effect the conversion $CH_4 \rightarrow CH_3OH$.[31,32,68,69] The analogy between the M_2O_2 "diamond-like" cores of Cu, Mn, and Fe complexes examined to date (including those at lower oxidation levels) is underscored by their topological similarities (Table 5). On the other hand, the apparently diverse roles of the various cores in dioxygen activation and generation processes implicate significant reactivity differences among them. Understanding the geometric and electronic structural bases for these differences remains an important research objective in bioinorganic chemistry.

Experimental Section

General Procedures. All reagents and solvents were obtained from commercial sources and used as received unless noted otherwise. Solvents were dried according to published procedures[70] and distilled under N_2 immediately prior to use. Dioxygen gas was dried by passing through two short columns of supported P_4O_{10} and Drierite. Labeled dioxygen ($^{18}O_2$, 99%) was obtained from Cambridge Isotopes, Inc., and used without further purification. All air-sensitive reactions were performed either in a Vacuum Atmospheres inert-atmosophere glovebox under a N_2 atmosphere or by using standard Schlenk and vacuum line techniques. The salts $[Cu(CH_3CN)_4]X$ ($X = ClO_4^-$, SbF_6^-, or $CF_3SO_3^-$) were prepared as described in the literature.[71] The ligands 1,4,7-triisopropyl-1,4,7-triazacyclononane (L^{iPr_3})[25] and 1,4,7-tribenzyl-1,4,7-triazacyclononane (L^{Bn_3})[26] were synthesized using published procedures. d_7-2-Bromopropane [$(CD_3)_3CDBr$, 98%] was purchased from Aldrich and used as received; d_7-benzyl chloride ($C_6D_5CD_2Cl$) was prepared by refluxing d_8-toluene (99%; Aldrich) with SO_2Cl_2 for ~30 min in the presence of a trace amount of benzoyl peroxide.[72] Deuterium incorporation was determined by integration of the residual proton signals in ^1H NMR spectra. Elemental analyses were performed by Atlantic Microlabs of Norcross, GA.

Safety Note. ***Caution!*** *Perchlorate salts of metal complexes with organic ligands are potentially explosive. Only small amounts of material should be prepared, and these should be handled with great care.*

Physical Methods. IR spectra were recorded on a Mattson Polaris FTIR spectrometer, as KBr pellets or neat films between NaCl plates. Low-temperature UV−vis spectra were recorded on a Hewlett-Packard HP8452A diode array spectrophotometer (190−820 nm scan range) by using a custom manufactured vacuum dewar equipped with quartz windows. Low temperatures were achieved by adding liquid nitrogen to a MeOH bath. The bath temperature was monitored by using a resistance thermocouple probe (Fluke 51 K/J Thermometer). Resonance Raman spectra were collected on a Spex 1403 spectrometer interfaced with a DM3000 data collection system using a Spectra-Physics Model 2030-15 argon ion laser. The spectra were obtained at 77 K using a backscattering geometry; samples were frozen onto a gold-plated copper cold finger in thermal contact with a dewar containing liquid nitrogen. Raman frequencies were referenced to the intense features at 710 or 806 cm^{-1} from frozen CH_2Cl_2 or THF, respectively. ^1H and $^{13}C\{^1H\}$ NMR spectra were recorded on Varian VXR-300 or VXR-500 spectrometers. Chemical shifts (in ppm) are referenced to the residual solvent peak(s). EPR spectra were obtained by using a Bruker ESP300 spectrometer fitted with a liquid nitrogen finger dewar (77 K, ~9.4 GHz). Electrospray mass spectral data were collected using a Sciex API III mass spectrometer (Sciex, Thornhill, Ontario, Canada). Cold CH_2Cl_2 (<−40 °C; syringe cooled externally with dry ice) was introduced by a syringe infusion pump (Model 22, Harvard Apparatus, South Natick, MA) through a 76 mm internal diameter fused silica capillary line at flow rates of ~10 mL/min for about 5 min, and then the cold sample solution, which was prepared at −80 °C, was introduced. The instrument was scanned in 0.2-dalton steps, and signal averaging was used to enhance the signal-to-noise ratio. Routine low resolution electron impact mass spectra (LREIMS) were obtained on a Hewlett-Packard GCD series G1800A GC/MS equipped with a 30 m HP-5 (crosslinked 5% PhMe-silicone) column. Fast atom bombardment (FAB) mass spectra were determined using a VG 7070E-HF mass spectrometer with xenon gas ionization in a matrix of *m*-nitrobenzyl alcohol (MNBA). Electrochemical experiments were perfomed as previously described[37] using an EG&G Princeton Applied Research (PAR) VeraStat potentiostat driven by EG&G PAR Model 250 software.

X-ray absorption spectra (XAS) were collected at the Cu K-edge (~9.0 KeV) at the Cornell High Energy Synchrotron Source (CHESS, station C2) and the National Synchrotron Light Source (Brookhaven National Laboratory, station X9). The monochromator was calibrated using the 8993 eV peak in the spectrum of Cu foil. Data were obtained in transmission mode [$A_{exp} = \log(I_0/I_1)$] on samples comprised of microcrystalline solids dispersed in boron nitride (see below for sample preparation details). Data analysis was performed as previously described,[29] via a variation of the FABM ("fine adjustment based on models") procedure that uses theoretical amplitude and phase functions calculated according to a curved-wave formalism. The crystallographically characterized complexes $[Cu(O_2CCH_3)_2 \cdot H_2O]_2$,[73] $[Cu(CH_3CN)_4]ClO_4$,[74] and $[(TMEN)Cu(OH)]_2(Br)_2 \cdot H_2O$[56] were used to determine the empirical amplitude reduction factors (A) and shell-specific edge shifts (ΔE) employed to partially compensate for imperfections in the theoretical amplitude and phase functions. The viability of these empirical parameters was tested by using them to analyze EXAFS data for $[(L^{iPr_3}Cu)_2(OH)_2](X)_2$ (Table 6).

Manometry. Low temperature gas uptake experiments were performed by using an apparatus as described earlier.[75] A standard 25 mL Schlenk tube, used as the reaction vessel, was connected via its side arm and a short piece of rubber tubing through a glass "T" to a second Teflon stopcock, then to a three-way glass stopcock which was linked to both vacuum and dioxygen inlet lines. The powdered sample [Cu(I) starting material or calibration standard, Vaska's complex] was stored in a small flask connected to the Schlenk flask with a ground glass joint, initially isolated from the system with a Teflon stopcock. The system, including the Schlenk flask containing the solvent (CH_2Cl_2), was cooled to −75 °C using an isopropyl alcohol/dry ice bath and evacuated and refilled with dioxygen three times to ensure a pure dioxygen atmosphere. The system was then shut off from the gas/vacuum inlet with the Teflon stopcock, and the initial pressure was recorded after allowing equilibration at −75 °C for 30 min. The powdered sample was then opened and allowed to fall into the solvent in the Schlenk flask whereupon it started reacting immediately. The solution was kept at −75 °C and vigorously stirred with a magnetic stir bar for 4 h. The pressure change in the system was recorded until it stabilized. The moles of dioxygen gas absorbed were then calculated using the ideal gas law.

1,4,7-Triisopropyl(d_7)-1,4,7-triazacyclononane (d_{21}-L^{iPr_3}). This ligand was prepared as described in the literature[25] using d_7-2-bromopropane and was isolated as clear, colorless oil. Deuterium content: 99% ($-CD(CD_3)_2$), 96% ($-CD(CD_3)_2$). ^1H NMR (300 MHz, $CDCl_3$): δ 2.59 (s, 12H) ppm. $^{13}C\{^1H\}$NMR (75 MHz, $CDCl_3$): δ 53.6 (t, $^1J_{CD} = 19.4$ Hz), 52.8, 17.4 (br) ppm. LREIMS: *m/z* (rel intens) 276 [M^+, 1], 108 (100).

1,4,7-Tribenzyl(d_7)-1,4,7-triazacyclononane (d_{21}-L^{Bn_3}). This ligand was synthesized in a similar manner as described for L^{Bn_3},[26] except d_7-benzyl chloride was reacted with 1,4,7-triazacyclononane. The ligand was isolated as thick yellow oil which solidified upon standing. Deuterium content: 98% ($-CD_2C_6D_5$). ^1H NMR ($CDCl_3$, 300 MHz): δ 2.83 (s, 12H) ppm. $^{13}C\{^1H\}$ NMR ($CDCl_3$, 75 MHz): δ 55.3 ppm. FTIR (KBr, cm^{-1}): 2277 (C−D), 2165 (C−D), 2045 (C−D); HREIMS calcd for $C_{27}H_{12}D_{21}N_3$ 420.3993, found 420.4007.

1,4-Diisopropyl-7-(*p*-tolylsulfonyl)-1,4,7-triazacyclononane. 1-(*p*-Tolylsulfonyl)-1,4,7-triazacyclononane (5.08 g, 0.018 mol) and 2-bro-

(68) Shteinman, A. A. *FEBS Lett.* **1995**, *362*, 5−9.
(69) (a) Feig, A. L.; Lippard, S. J. *Chem. Rev.* **1994**, *94*, 759−805. (b) Liu, K. E.; Johnson, C. C.; Newcomb, M.; Lippard, S. J. *J. Am. Chem. Soc.* **1993**, *115*, 939−947.
(70) Perrin, D. D.; Armarego, W. L. F. *Purification of Laboratory Chemicals*; Pergamon Press: New York, 1988.
(71) Kubas, G. J. *Inorg. Synth.* **1979**, *19*, 90−92; **1990**, *28*, 68−70.
(72) Furness, B. S.; Hannaford, A. J.; Smith, P. W. G.; Tatchell, A. R. *Vogel's Textbook of Practical Organic Chemistry*; Longman Scientific & Technical: Essex, U.K., 1989; p 864.
(73) Brown, G. M.; Chidambaram, R. *Acta Crystallogr.* **1973**, *B29*, 2393−2403.
(74) Csöregh, I.; Kierkegaard, P.; Norrestam, R. *Acta Crystallogr.* **1975**, *B31*, 314−317.
(75) Ruggiero, C. E.; Carrier, S. M.; Antholine, W. E.; Whittaker, J. W.; Cramer, C. J.; Tolman, W. B. *J. Am. Chem. Soc.* **1993**, *115*, 11285−11298.

mopropane (8.84 g, 0.072 mol) were combined in degassed CH_3CN (20 mL). Na_2CO_3 (8.04 g) was added as a solid to the above colorless solution, and the resultant mixture was heated at reflux under N_2 for 18 h. The then yellow mixture was filtered from excess Na_2CO_3, and the solid washed with fresh CH_3CN. The combined filtrates were evaporated under reduced pressure to yield a yellow oil with a small amount of a white solid. The residue was redissolved in $CHCl_3$ (20 mL) and then washed with 1 M NaOH. The organic layer was removed, and the aqueous phase was extracted with $CHCl_3$ (3 × 10 mL). The combined $CHCl_3$ layers were dried ($MgSO_4$), and the solvent removed under reduced pressure to yield 5.94 g (90%) of a tan solid. Mp: 58−59 °C. ^{1}H NMR ($CDCl_3$, 500 MHz): δ 7.66 (d, J = 8.0 Hz, 2H), 7.26 (d, J = 8.0 Hz, 2H), 3.28−3.26 (m, 4H), 2.85−2.83 (m, 4H), 2.75 (septet, J = 6.5 Hz, 2H), 2.43 (s, 4H), 2.39 (s, 3H), 0.91 (d, J = 6.5 Hz, 12H) ppm. ^{13}C{^{1}H} NMR ($CDCl_3$, 125 MHz): δ 142.54, 136.29, 129.33, 126.94, 53.53, 53.51, 52.11, 50.17, 21.28, 18.08 ppm. LRE-IMS: *m/z* 366 [M^+, 1], 141 (100). Anal. Calcd for $C_{19}H_{33}N_3O_2S$: C, 62.09; H, 9.05; N, 11.43. Found: C, 61.95; H, 9.05; N, 11.43.

1,4-Diisopropyl-1,4,7-triazacyclononane (L^{iPr_2H}). A mixture of 1,4-diisopropyl-7-(*p*-tolylsulfonyl)-1,4,7-triazacyclononane (5.94 g, 0.016 mol) and 18 M H_2SO_4 (20 mL) was heated at 120 °C for 18 h under N_2. After cooling to room temperature, the dark mixture was poured into crushed ice (100 g), and the resultant dark mixture brought to pH > 11 with aqueous NaOH. The heterogenous mixture was extracted with $CHCl_3$ until the organic extracts were colorless (ca. 500 mL total). The $CHCl_3$ solution of the product was dried ($MgSO_4$), and the solvent removed under reduced pressure to yield 3.25 g (94%) of an amber oil. While suitable for further synthetic use, the crude product may be purified by Kugelrohr distillation (80−82 °C, 0.01 Torr) to yield a colorless oil, 2.60 g (75%). ^{1}H NMR ($CDCl_3$, 300 MHz): δ 3.36 (br s, 1H), 2.74 (septet, J = 6.6 Hz, 2H), 2.57−2.53 (m, 4H), 2.47−2.43 (m, 4H), 2.36 (s, 4H), 0.88 (d, J = 6.6 Hz, 12H) ppm. ^{13}C{^{1}H} NMR ($CDCl_3$, 75 MHz) δ 52.72, 48.90, 47.86, 47.03, 18.49 ppm. FTIR (neat): 3370 (br, ν_{NH}), 2966, 2931, 2867, 1680, 1490, 1487, 1462, 1458, 1437, 1382, 1360, 1319, 1303, 1264, 1253, 1190, 1169, 1149, 1132, 1116, 1108, 1093, 1040, 751, 714, 708, 704, 701 cm^{-1}. HRCIMS (NH_3): calcd for $C_{12}H_{28}N_3$ (M + H) 214.2283, found 214.2277. Anal. Calcd for $C_{12}H_{27}N_3$: C, 67.55; H, 12.75; N, 19.69. Found: C, 66.79; H, 12.65; N, 19.69.

1-Benzyl-4,7-diisopropyl-1,4,7-triazacyclononane (L^{iPr_2Bn}). To a solution of 1,4-diisopropyl-1,4,7-triazacyclononane (0.22 g, 1.03 mmol) in CH_3CN (10 mL) was added benzyl chloride (0.13 g, 1.03 mmol). After addition of Na_2CO_3 (∼0.5 g) and tetrabutylammonium bromide (10 mg), the mixture was heated at reflux under N_2 for 18 h. After cooling to room temperature, the mixture was filtered, the filter cake washed with $CHCl_3$ (10 mL), and the combined filtrates dried ($MgSO_4$). Removal of solvent under reduced pressure afforded the crude product (0.22 g, 70%) which was suitable for metal complex synthesis; further purification was effected by a vacuum distillation (bp 116 °C, 0.01 Torr). ^{1}H NMR ($CDCl_3$, 300 MHz): δ 7.34−7.27 (m, 5H), 3.64 (s, 2H), 2.90−2.83 (m, 4H), 2.88 (septet, J = 6.6 Hz, 2H), 2.59−2.62 (m, 4H), 2.60 (s, 4H), 0.94 (d, J = 6.6 Hz, 12H) ppm. ^{13}C{^{1}H} NMR ($CDCl_3$, 75 MHz): δ 140.74, 128.9, 128.0, 126.5, 62.2, 55.3, 54.8, 52.7, 52.3, 18.3 ppm. FTIR (neat): 3084, 3064, 3027, 2964, 2932, 2795, 1945, 1873, 1813, 1681, 1607, 1496, 1456, 1381, 1361, 1307, 1262, 1173, 1156, 1116, 1096, 1030, 1001, 975, 910, 780, 731, 699 cm^{-1}; HREIMS: calcd for $C_{19}H_{33}N_3$ 303.2674, found 303.2683. Anal. Calcd for $C_{19}H_{33}N_3$: C, 75.19; H, 10.96; N, 13.85. Found: C, 75.02; H, 10.94; N, 13.82.

[L^{iPr_3}Cu(CH_3CN)]X (X = ClO_4^-, $CF_3SO_3^-$, SbF_6^-). These complexes were prepared as described in the literature for [L^{iPr_3}Cu(CH_3CN)]PF_6,[37] substituting the appropriate [Cu(CH_3CN)$_4$]X salt, and were isolated as colorless solids in 85−95% yield. **(X = ClO_4^-).** ^{1}H NMR (300 MHz, CD_2Cl_2): δ 3.08 (septet, J = 6.6 Hz, 3H), 2.85−2.77 (m, 6H), 2.59−2.51 (m, 6H), 2.24 (s, 3H), 1.21 (d, J = 6.6 Hz, 18H) ppm. ^{13}C{^{1}H} NMR (75 MHz, CD_2Cl_2): δ 58.5, 51.2, 19.9 ppm. FTIR (KBr, cm^{-1}): 2267 (C≡N), 1090 (ClO_4^-), 623 (ClO_4^-). Anal. Calcd for $C_{17}H_{36}N_4CuClO_4$: C, 44.44; H, 7.90; N, 12.19. Found: C, 44.29; H, 7.77; N, 11.94. **(X = $CF_3SO_3^-$).** FTIR (KBr, cm^{-1}): 2267 (C≡N), 1225 ($CF_3SO_3^-$), 1150 ($CF_3SO_3^-$), 1029 ($CF_3SO_3^-$), 637 ($CF_3SO_3^-$). Anal. Calcd for $C_{18}H_{36}N_4CuF_3O_3S$: C, 42.47; H, 7.13; N, 11.00. Found: C, 42.86; H, 7.43; N, 10.18. **(X = SbF_6^-).** FTIR (KBr, cm^{-1}): 2267 (C≡N), 657 (SbF_6^-). Anal. Calcd for $C_{17}H_{36}N_4CuSbF_6$: C, 34.34; H, 6.11; N, 9.43. Found: C, 34.43; H, 6.10; N, 9.43.

[L^{iPr_3}Cu(CH_3CN)]BPh_4. A solution of CuCl (0.20 g, 2.00 mmol) in CH_3CN (5 mL) was treated with a solution of L^{iPr_3} (0.52 g, 2.04 mmol) in THF (3 mL). After stirring the colorless solution for 30 min, a solution of $NaBPh_4$ (0.68 g, 1.99 mmol) in CH_3CN (5 mL) was added, causing the precipitation of NaCl. After stirring for an additional 30 min the mixture was filtered through a pad of Celite and the filtrate treated with Et_2O (20 mL). Storage at −20 °C caused the deposition of colorless plate crystals of the product (1.09 g, 80%). ^{1}H NMR (500 MHz, CD_2Cl_2): δ 7.34−7.32 (m, 8H), 7.04 (t, J = 6.5 Hz, 8H), 6.89 (t, J = 7.5 Hz, 4H), 3.05 (septet, J = 6.5 Hz, 3H), 2.79−2.72 (m, 6H), 2.48−2.42 (m, 6H), 1.94 (s, 3H), 1.20 (d, J = 6.5 Hz, 18H) ppm. ^{13}C{^{1}H} NMR (125 MHz, CD_2Cl_2): δ 164.6, 135.4, 126.2, 126.1, 122.2, 58.6, 51.2, 20.0, 3.2 ppm. FTIR (KBr, cm^{-1}): 2265 (C≡N), 734 (BPh_4^-), 704 (BPh_4^-). Anal. Calcd for $C_{41}H_{56}N_4BCu$: C, 72.50; H, 8.31; N, 8.25. Found: C, 72.13; H, 8.33; N, 8.33.

[L^{iPr_3}Cu(CH_3CN)][B($C_6H_3(CF_3)_2$)$_4$]. Na[B($C_6H_3(CF_3)_2$)$_4$][36] (0.35 g, 0.40 mmol) was dissolved in Et_2O (2 mL), and then diluted with CH_2Cl_2 (3 mL). A solution of [L^{iPr_3}Cu(CH_3CN)]SbF_6 (0.24 g, 0.40 mmol) in CH_2Cl_2 (3 mL) was added dropwise with stirring to the solution of Na[B($C_6H_3(CF_3)_2$)$_4$] causing the immediate deposition of a colorless precipitate ($NaSbF_6$). The mixture was stirred for 30 min and then filtered through a pad of Celite. The solvent was removed from the nearly colorless filtrate and the resultant residue was extracted with Et_2O (5 mL). Evaporation of the solvent under reduced pressure yielded the product as a light tan solid (0.24 g, 50%). ^{1}H NMR (300 MHz, CD_3CN): δ 7.72−7.70 (br m, 12H), 3.06 (septet, J = 6.6 Hz, 3H), 2.84−2.74 (m, 6H), 2.59−2.48 (m, 6H), 1.19 (d, J = 6.6 Hz, 12H) ppm. FTIR (KBr, cm^{-1}): 2277 (C≡N). Anal. Calcd for $C_{49}H_{48}N_4BCuF_{24}$: C, 48.11; H, 3.96; N, 4.58. Found: C, 47.70; H, 4.07; N, 4.64.

[d_{21}-L^{iPr_3}Cu(CH_3CN)]ClO_4. This complex was prepared in an analogous fashion to [L^{iPr_3}Cu(CH_3CN)]ClO_4 except using d_{21}-L^{iPr_3} on 0.733 mmol scale (0.31 g, 90%). ^{1}H NMR (300 MHz, CD_2Cl_2): δ 2.74−2.84 (m, 6H), 2.50−2.59 (m, 6H), 2.22 (s, 3H) ppm. ^{13}C{^{1}H} NMR (75 MHz, CD_2Cl_2): δ 57.7 (t, J_{CD} = 21 Hz), 51.1, 18.9 (br), 3.4 ppm. FTIR (KBr, cm^{-1}): 2267 (C≡N), 2227 (C−D), 2136 (C−D), 2070 (C−D), 1093 (ClO_4^-), 623 (ClO_4^-).

[L^{iPr_3}Cu(CO)]SbF_6. Solid [L^{iPr_3}Cu(CH_3CN)]SbF_6 (0.20 g, 0.33 mmol) was dissolved in THF (10 mL) in a Schlenk flask. Carbon monoxide was then bubbled through the solution for 10 min at room temperature. Addition of Et_2O (10 mL) to the colorless solution yielded a white precipitate, which was recrystallized from CH_2Cl_2/Et_2O (0.18 g, 92%). ^{1}H NMR (300 MHz, $CDCl_3$): δ 3.23 (septet, J = 6.6 Hz, 3H), 2.98−2.87 (m, 6H), 2.80−2.71 (m, 6H), 1.27 (d, J = 6.6 Hz, 18H) ppm. ^{13}C{^{1}H} NMR (75 MHz, $CDCl_3$): δ 206.8, 59.1, 51.4, 20.1 ppm. FTIR (KBr, cm^{-1}): 2067 (C≡O), 658 (SbF_6^-). Anal. Calcd for $C_{16}H_{33}N_3OCuSbF_6$: C, 32.98; H, 5.71; N, 7.21. Found: C, 33.00; H, 5.71; N, 7.14.

[L^{Bn_3}Cu(CH_3CN)]X (X = ClO_4^-, SbF_6^-, and $CF_3SO_3^-$). To a stirred solution of 0.20 g (0.50 mmol) of L^{Bn_3} in THF (2 mL) was added [Cu(CH_3CN)$_4$]X (X = ClO_4^-, SbF_6^- and $CF_3SO_3^-$) (0.50 mmol). After stirring the mixture for 10 min, Et_2O (∼5 mL) was added to the light yellow solution with vigorous stirring. The off-white precipitate that formed was collected by filtration, washed with Et_2O and dried under vacuum or under a stream of nitrogen. Recrystallization of this solid from THF/ether or CH_2Cl_2/ether yielded the products as off-white microcrystals. **(X = ClO_4^-).** Yield: 0.28 g, 93%. ^{1}H NMR (CD_2Cl_2, 300 MHz): δ 7.36−7.32 (m, 15H), 3.85 (s, 6H), 2.75−2.65 (m, 6H), 2.59−2.49 (m, 6H), 2.36 (s, 3H) ppm. ^{13}C{^{1}H} NMR (CD_2Cl_2, 75 MHz): δ 135.1, 131.2, 128.8, 64.3, 52.4 ppm. FTIR (KBr, cm^{-1}): 2270 (C≡N), 1098 (ClO_4^-), 623 (ClO_4^-). FAB-MS (MNBA): *m/z* (rel intens) 561 {[L^{Bn_3}Cu(ClO_4) − H]$^+$, 5} 462 {[L^{Bn_3}Cu]$^+$, 100}. Anal. Calcd for $C_{29}H_{36}N_4CuClO_4$: C, 57.79; H, 6.03; N, 9.30. Found: C, 57.51; H, 5.94; N, 9.28. **(X = SbF_6^-).** Yield: 0.33 g, 90%. FTIR (KBr, cm^{-1}): 2267 (C≡N), 657 (SbF_6^-), 520. FAB-MS (MNBA) *m/z* (rel intens) 699 {[L^{Bn_3}Cu(SbF_6) − H]$^+$, 1}, 462 {[L^{Bn_3}Cu]$^+$, 100}. Anal. Calcd for $C_{29}H_{36}N_4CuSbF_6$: C, 47.15; H, 4.92; N, 7.59. Found: C, 47.56; H, 5.10; N, 7.57. **(X = $CF_3SO_3^-$).** Yield: 0.28 g, 85%. FTIR (KBr, cm^{-1}): 1252 ($CF_3SO_3^-$), 1161 ($CF_3SO_3^-$), 1030 ($CF_3SO_3^-$), 638

($CF_3SO_3^-$). Anal. Calcd for $C_{30}H_{36}N_4CuSO_3F_3$: C, 55.20; H, 5.56; N, 8.59. Found: C, 55.51; H, 5.54; N, 8.64.

[d_{21}-L^{Bn_3}Cu(CH_3CN)]X (X = ClO_4^- and SbF_6^-). These compounds were prepared in a manner analogous to that described for [L^{Bn_3}-Cu(CH_3CN)]X (X = ClO_4^- and SbF_6^-) except d_{21}-L^{Bn_3} (0.2 g, 0.475 mmol) was used. **(X = ClO_4^-).** Yield 0.27 g, 91%. ^{1}H NMR (CD_2Cl_2, 300 MHz): δ 2.74−2.64 (m, 6H), 2.56−2.46 (m, 6H), 2.36 (s, 3H) ppm. ^{13}C{^{1}H} NMR (CD_2Cl_2, 75 MHz): δ 52.2 ppm. FTIR (KBr, cm^{-1}): 2273 (C≡N), 2247 (C−D), 2209 (C−D), 2149 (C−D), 2102 (C−D), 2067 (C−D), 2021 (C−D), 1098 (ClO_4^-), 622 (ClO_4^-). FAB-MS (MNBA): *m/z* (rel intens) 582 {[d_{21}-L^{Bn_3}Cu(ClO_4) − H]$^+$, 5}, 483 {[d_{21}-L^{Bn_3}Cu]$^+$, 100}. Anal. Calcd for $C_{29}H_{15}D_{21}N_4CuClO_4$: C, 55.83; H/D, 5.81; N, 8.99. Found: C, 55.51; H/D, 5.94; N, 9.08. **(X = SbF_6^-).** Yield: 0.32 g, 88%. FTIR (KBr, cm^{-1}): 2278 (C≡N), 2204 (C−D), 2155 (C−D), 2100 (C−D), 2064 (C−D), 655 (SbF_6^-). FAB-MS (MNBA): *m/z* (rel intens) 720 {[d_{21}-L^{Bn_3}Cu(SbF_6) − H]$^+$, 3}, 483 {[d_{21}-L^{Bn_3}Cu]$^+$, 100}. Anal. Calcd for $C_{29}H_{15}D_{21}N_4CuSbF_6$: C, 45.83; H/D, 4.78; N, 7.38. Found: C, 46.06; H, 4.95; N, 7.22.

[L^{Bn_3}Cu(CO)]ClO_4. Solid [L^{Bn_3}Cu(CH_3CN)]ClO_4 (0.10 g, 0.17 mmol) was dissolved in CH_2Cl_2 (5 mL) in a Schlenk flask. Carbon monoxide was then bubbled through the solution for 10 min at room temperature. A white precipitate formed while bubbling the CO; Et_2O (10 mL) was then added to complete the precipitation. The white microcrystalline product was collected, washed with CH_2Cl_2/Et_2O, and then dried under vacuum (0.83 g, 85%). ^{1}H NMR (500 MHz, CD_2Cl_2): δ 7.37−7.34 (m, 15H), 3.94 (s, 6H), 2.92−2.86 (m, 6H), 2.84−2.79 (m, 6H) ppm. FTIR (KBr, cm^{-1}): 2084 (C≡O), 1089 (ClO_4^-), 622 (ClO_4^-). Anal. Calcd for $C_{28}H_{33}N_3OCuClO_4$: C, 57.03; H, 5.65; N, 7.13. Found: C, 56.28; H, 5.56; N, 7.01.

[L^{iPr_2Bn}Cu(CH_3CN)]ClO_4. This compound was prepared in a manner analogous to that described for [L^{Bn_3}Cu(CH_3CN)]ClO_4^- except L^{iPr_2Bn} (0.2 g, 0.66 mmol) was used instead of L^{Bn_3}. Yield: 0.31 g, 91%. ^{1}H NMR (acetone-d_6, 300 MHz): δ 7.64−7.61 (m, 2H), 7.45−7.35 (m, 3H), 4.01 (s, 2H), 3.06 (septet, J = 6.6 Hz, 2H); 3.05−2.95 (m, 2H), 2.90−2.50 (overlapping multiplets, 10H), 2.43 (br s, 3H), 1.20 (d, J = 6.6 Hz, 6H), 1.17 (d, J = 6.6 Hz, 6H) ppm. ^{13}C{^{1}H} NMR (acetone-d_6, 75 MHz): δ 132.2, 129.0, 64.8, 58.5, 54.6, 51.8, 49.8, 20.3, 19.3 ppm. FTIR (KBr, cm^{-1}): 2263 (C≡N), 1090 (ClO_4^-), 622 (ClO_4^-). Anal. Calcd for $C_{21}H_{36}N_4CuClO_4$: C, 49.70; H, 7.15; N, 11.04. Found: C, 50.05; H, 7.18; N, 10.93.

[L^{iPr_2Bn}Cu(CO)]ClO_4. This compound was prepared in a manner analogous to that described for [L^{iPr_3}Cu(CO)]ClO_4 and recrystallized from THF/Et_2O. Yield: 0.088 g, 90%. ^{1}H NMR (500 MHz, $CDCl_3$) δ 7.40−7.37 (m, 4H), 4.00 (s, 2H), 3.10 (septet, J = 6.5 Hz, 2H), 3.05−2.98 (m, 4H), 2.89−2.79 (m, 4H), 2.76−2.67 (m, 4H), 1.16−1.13 (two overlapping doublets, J = 6.6 Hz, 12H) ppm. ^{13}C{^{1}H} NMR (125 MHz, $CDCl_3$): δ 134.8, 131.4, 129.1, 128.8, 65.2, 59.0, 54.7, 51.8, 50.0, 20.5, 19.8 ppm. FTIR (KBr, cm^{-1}): 2069 (C≡O), 1091 (ClO_4^-), 622 (ClO_4^-). Anal. Calcd for $C_{22}H_{36}N_3OCuClO_4$: C, 48.67; H, 6.74; N, 8.52. Found: C, 48.13; H, 6.62; N, 8.30.

[(LCu)$_2$(μ-O)$_2$](X)$_2$ (L = L^{Bn_3}, L^{iPr_3}, and L^{iPr_2Bn}; X = ClO_4^-, SbF_6^-, and $CF_3SO_3^-$). Solid [LCu(CH_3CN)]X (∼0.20 g) was placed in a Schlenk flask and cooled to −80 °C. Dry CH_2Cl_2 (10 mL) (L^{Bn_3} or L^{iPr_2Bn}) or THF (L^{iPr_3}) was then injected into the Schlenk flask and dry dioxygen was then bubbled through the cold solution for 15 min. The initially colorless solution became deep orange-brown. Spectroscopic characterization of these compounds were performed at a low temperature (∼−80 °C) immediately after generation. Low-temperature ^{1}H and ^{13}C NMR spectra were obtained at −75 °C using the Varian VXR-500 spectrometer as follows. In the glovebox, ∼ 0.03 g of [L^{Bn_3}Cu-(CH_3CN)]ClO_4 was dissolved in ∼0.5 mL CD_2Cl_2 or in 0.6 mL of d_6-acetone/CD_2Cl_2 (2:1) solvent mixture in a NMR tube capped with a septum. After removal from the glovebox, the tube was immersed into a cold bath maintained at −80 °C and O_2 was then bubbled in through a needle for 15 min. After oxygenation, the dark brown mixture was purged with N_2 to remove excess O_2. The NMR tube was then transferred to the precooled (−75 °C) probe of the spectrometer. EPR (CH_2Cl_2, 9.4 GHz, 77 K): silent. **(L = L^{Bn_3}).** ^{1}H NMR (-75 °C, CD_2Cl_2, 500 MHz) δ 7.44−7.36 (m, 30H), 4.57 (s, 12H), 3.54 (br, s,12H), 2.50 (br s, 12H) ppm. ^{13}C{^{1}H} NMR (−75 °C, CD_2Cl_2, 75 MHz): δ 134.6, 132.1, 131.0, 128.9, 59.7 ppm. ^{1}H NMR [−75 °C, d_6-acetone/CD_2Cl_2 (2:1), 500 MHz]: δ 7.54−7.45 (m, 30H), 4.87 (s, 12H), 3.71 (br s,12H), 2.73 (br s, 12H) ppm. ^{13}C{^{1}H} NMR (−75 °C, d_6-acetone/CD_2Cl_2 (2:1), 75 MHz): δ 133.0, 132.3, 128.9, 59.5, 51.0 (br) ppm. Samples of [(d_{21}-L^{Bn_3}Cu)$_2$(μ-O)$_2$](X)$_2$ (X = ClO_4^-, SbF_6^-, and $CF_3SO_3^-$) were prepared similarly. NMR characterization was performed for the case X = ClO_4^-. ^{1}H NMR (−75 °C, CD_2Cl_2, 500 MHz): δ 3.54 (br, s, 12H), 2.48 (br s, 12H) ppm. ^{1}H NMR [−75 °C, d_6-acetone/CD_2Cl_2 (2:1), 500 MHz]: δ 3.70 (br s,12H), 2.73 (br s, 12H) ppm. electrospray-MS (CH_2Cl_2, ∼−40 °C): *m/z* (rel intens) (X = ClO_4^-) 1099 {[(d_{21}-L^{Bn_3}Cu)$_2$(μ-O)$_2$(ClO_4)]$^+$, 55}, 525 {[d_{21}-L^{Bn_3}Cu(CH_3CN)]$^+$, 100}; (X = SbF_6^-) positive ion 1235 {[(d_{21}-L^{Bn_3}Cu)$_2$(μ-O)$_2$(SbF_6)]$^+$, 20}, 525 {[d_{21}-L^{Bn_3}Cu(CH_3CN)]$^+$, 100}; negative ion 1707 {[(d_{21}-L^{Bn_3}Cu)$_2$(μ-O)$_2$(SbF_6)$_3$]$^-$, 100}.

Preparation of [(LCu)$_2$(μ-O)$_2$](X)$_2$ Samples for EXAFS Experiments. A solution of [L^{iPr_3}Cu(CH_3CN)]ClO_4 (0.10 g) in THF (10 mL) was cooled to −80 °C and oxygenated by purging with dry O_2 for 1 h, causing a color change from colorless to deep orange-brown and the precipitation of an orange-brown solid. While stirring vigorously, cold (−80 °C) Et_2O (30 mL) was added to complete the precipitation of the complex. After the solid was allowed to settle, the supernatant was removed with a frozen pipet. The dispersant boron nitride (precooled to −80 °C) was then added to the moist solid and the mixture homogenized with a frozen spatula. An additional amount of cold diethyl ether (2 mL) was then added to facilitate transfer of the mixture to the sample holder, which was frozen in a liquid N_2 bath. The Et_2O suspension of the sample mixture was taken up in a frozen glass pipette and transferred to the frozen sample holder where the sample immediately froze. After the sample holder was loaded, the sample was covered with a window of mylar film and stored below 100 K until subjected to X-ray analysis. A similar method was used to prepare samples of [(L^{Bn_3}Cu)$_2$(μ-O)$_2$](ClO_4)$_2$, which was initially prepared in cold acetone and precipitated with cold Et_2O.

[(L^{iPr_2H}Cu)$_2$(μ-OH)$_2$](BPh$_4$)$_2$. A solution of [L^{iPr_3}Cu(CH_3CN)]ClO_4 (0.13 g, 0.28 mmol) in THF (10 mL) was cooled to −80 °C and oxygenated by purging with dry O_2 for 1 h; excess O_2 was then removed by purging with N_2 for 30 min. The heterogenous mixture was then allowed to warm to room temperature, causing a color change from orange-brown to blue-green and the precipitation of a green solid. The solid was redissolved in CH_3CN and the solution treated with excess $NaBPh_4$ (0.50 g). The resultant mixture was stored at −20 °C overnight, causing the deposition of blue-green microcrystals (0.10 g, 30%). Recrystallization of this solid from THF/CH_3CN at −20 °C produced a small number of blue crystals of [(L^{iPr_2H}Cu)$_2$(μ-OH)$_2$]-(BPh$_4$)$_2$·2THF suitable for crystallographic analysis. EPR (1:1 CH_3-CN/toluene, 9.4 GHz, 77 K): silent. FTIR (KBr, cm^{-1}): 3416 (br, O−H), 3275 (N−H), 710 (BPh_4^-). Electrospray-MS (CH_3CN) *m/z* 908 {[(L^{iPr_2H}Cu)$_2$(OH)$_2$(BPh$_4$)]$^+$, 100}.

[(L^{Bn_3}Cu)$_2$(μ-OH)$_2$](ClO_4)$_2$·DMF·H$_2$O. A solution of [(L^{Bn_3}Cu)$_2$-(μ-O)$_2$](ClO_4)$_2$ in CH_2Cl_2 at −80 °C was prepared as described above [0.10 g, 0.17 mmol scale of Cu(I) precursor]. After removing excess oxygen by purging nitrogen at −80 °C for 15 min, the solution was warmed to room temperature. The orange-brown solution turned blue-green at room temperature, whereupon a blue-green solid precipitated, leaving a green filtrate. The blue-green precipitate was then recrystallized by diffusing methanol into DMF solution at room temperature. After ∼48 h blue crystals were separated, washed with methanol and air dried (0.06 g, 60%). FTIR (KBr, cm^{-1}): 3574 (OH), 3444 (br, H_2O), 1662 (C═O, DMF), 1100 (ClO_4^-), 623 (ClO_4^-). UV−vis (DMF): (λ_{max}, nm (ϵ, M^{-1} cm^{-1})): 622 (190), 292 (3800). EPR (DMF, 9.4 GHz, 77 K): silent. electrospray-MS (DMF): *m/z* positive ion 1059 {[(L^{Bn_3}Cu)$_2$(OH)$_2$(ClO_4)]$^+$, 28}, 521 (100); negative ion 1257 {[(L^{Bn_3}Cu)$_2$(OH)$_2$(ClO_4)$_3$]$^-$, 38}, 721 (100). Anal. Calcd for $C_{57}H_{77}N_7Cu_2Cl_2O_{11}$: C, 54.84; H, 6.22; N, 7.86. Found: C, 54.68; H, 6.06; N, 7.66.

[(L^{Bn_3}Cu)(L^{Bn_2H}Cu)(μ-OH)$_2$](CF_3SO_3)$_2$·2(CH_3)$_2$CO. Following a similar methodology as described above, when an orange-brown solution of [(L^{Bn_3}Cu)$_2$(μ-O)$_2$](CF_3SO_3)$_2$ warmed slowly from −80 °C to room temperature under a positive dinitrogen flow, a blue-green solution resulted. A blue-green solid was isolated from this mixture by the addition of excess Et_2O. Recrystallization of this solid from acetone/Et_2O at room temperature yielded a small number of blue-green crystals suitable for X-ray crystallography. FTIR (KBr, cm^{-1}): 3573 (O−H), 3292 (N−H), 1253 ($CF_3SO_3^-$), 1160 ($CF_3SO_3^-$), 1030 ($CF_3SO_3^-$), 639 ($CF_3SO_3^-$). EPR (1:1 CH_3CN/toluene, 9.4 GHz, 77 K): silent.

$[(L^{iPr_2Bn}Cu)_2(\mu\text{-}OH)_2](CF_3SO_3)_2$. Following a similar methodology as described above, when an orange-brown solution of $[(L^{iPr_2Bn}Cu)_2(\mu\text{-}O)_2](CF_3SO_3)_2$ warmed slowly from −80 °C to room temperature under a positive dinitrogen flow, a blue-green solution with a blue-green precipitate resulted. The blue-green precipitate was collected and recrystallized by diffusing Et_2O into a DMF solution at room temperature (0.043 g, 45%). FTIR (KBr, cm^{-1}): 3606 (OH), 1265 ($CF_3SO_3^-$), 1160 ($CF_3SO_3^-$), 1031 ($CF_3SO_3^-$), 636 ($CF_3SO_3^-$). EPR (DMF, 9.4 GHz, 77 K): silent. UV−vis (DMF) (λ_{max}, nm (ϵ, M^{-1} cm^{-1})): 360 (sh, 2200), 650 (200). Anal. Calcd for $C_{40}H_{68}N_6Cu_2F_6S_2O_8$: C, 45.10; H, 6.44; N, 7.89. Found: C, 44.29; H, 6.33; N, 7.99.

Crossover Experiment. Equimolar amounts of the bis(μ-hydroxo)-dicopper(II) compounds $[(L^{Bn_3}Cu)_2(\mu\text{-}OH)_2](SbF_6)_2$ and $[(d_{21}\text{-}L^{Bn_3}Cu)_2(\mu\text{-}OD)_2](SbF_6)_2$ in CH_2Cl_2 were mixed at room temperature. After stirring for 30 min this mixture was injected to an electrospray-MS detector at room temperature. Electrospray MS (CH_2Cl_2): *m/z* (rel intens) positive ion 1197 $\{[(L^{Bn_3}Cu)_2(\mu\text{-}OH)_2(SbF_6)]^+, 30\}$, 1218 $\{[(d_{21}\text{-}L^{Bn_3}CuOD)(L^{Bn_3}CuOH)(SbF_6)]^+, 60\}$, 1237 $\{[(d_{21}\text{-}L^{Bn_3}Cu)_2(\mu\text{-}OD)_2(SbF_6)]^+, 35\}$; negative ion 1667 $\{[(L^{Bn_3}Cu)_2(\mu\text{-}OH)_2(SbF_6)_3]^-, 52\}$, 1689 $\{[(d_{21}\text{-}L^{Bn_3}CuOD)(L^{Bn_3}CuOH)(SbF_6)_3]^-, 100\}$, 1709 $\{[(d_{21}\text{-}L^{Bn_3}Cu)_2(\mu\text{-}OD)_2(SbF_6)_3]^-, 55\}$.

X-ray Crystallography. $[(d_{21}\text{-}L^{Bn_3}Cu)_2(\mu\text{-}O)_2](SbF_6)_2\cdot 7(CH_3)_2CO\cdot 2CH_3CN$. Crystals were grown by storing a solution of the complex prepared by oxygenation of $[d_{21}\text{-}L^{Bn_3}Cu(CH_3CN)]ClO_4$ in 1:1 $CH_2Cl_2/(CH_3)_2CO$ at −80 °C. A dark brown rectangular-shaped crystal was mounted to the side of a glass capillary at low temperature (< −40 °C) using a locally designed cold stage and then transferred to the goniometer of a Siemens SMART system, with the cryogenic stream set to 123(2) K for data collection. An initial set of cell constants was calculated from 354 reflections harvested from three sets of 30 frames. Final cell constants were calculated from a set of 6155 strong reflections from the data collection. A hemisphere collection involves the survey of a randomly oriented region of reciprocal space to the extent of 1.3 hemispheres to a resolution of 0.84 Å. Three major swaths of frames were collected with 0.30° steps in ω. A semiempirical absorption correction afforded minimum and maximum transmission factors of 0.624 and 0.871, respectively. See Table 2 for additional crystal and refinement information.

The space groups *Cc* or *C*2/*c* were determined based on systematic absences. Intensity statistics favored neither one. A successful direct-methods solution was calculated in *Cc* which provided most non-hydrogen atoms from the *E*-map. The structure was transformed into the centrosymmetric space group *C*2/*c* after checking with MISSYM.[76] Several full-matrix least squares/difference Fourier cycles were performed which located the remainder of the non-hydrogen atoms. All non-hydrogen atoms were refined with anisotropic displacement parameters. All hydrogen or deuterium atoms were placed in idealized positions and were refined as riding atoms with relative (1.2 times host for methylene, 1.5 times host for methyl) isotropic displacement parameters. All calculations were performed using SGI INDY R4400-SC or Pentium computers with the SHELXTL V5.0 program suite.[77]

The asymmetric unit contains one half of the dimeric cation as well as CH_3CN and 3.5 $(CH_3)_2CO$ solvent molecules and a rotationally disordered SbF_6^- counterion (disordered 7:1). Copious distance restraints were placed on the solvent molecules, the SbF_6^- counterions, and the phenyl groups of the cation to force these units to conform their respective average substructures. Additionally, the anisotropic displacement parameters for these were restrained to better fit rigid body motion. The residual electron density in the final difference Fourier map was located close to the disordered SbF_6^-. Drawings of the cation appear in Figures 4 and 8, and selected bond lengths and angles are presented in Table 3. Full details of the structure determination, including tables of bond lengths and angles, atomic positional parameters, and final thermal parameters for non-hydrogen atoms, are given in the Supporting Information.

$[(L^{Bn_3}Cu)(L^{Bn_2H}Cu)(\mu\text{-}OH)_2](CF_3SO_3)_2\cdot 2(CH_3)_2CO$. A blue-green plate-like crystal of the compound was attached to a glass fiber with heavy-weight oil and transferred to the goniometer of the Siemens SMART system, with cryogenic stream set to 173(2) K for data collection. Data collection was performed as described above. Important crystallographic information is given in Table 2. The space group $P2_1/n$ was determined on the basis of systematic absences and intensity statistics. A successful direct-methods solution was calculated which provided most non-hydrogen atoms from the *E*-map. Several full-matrix least squares/difference Fourier cycles were performed which located the remainder of the non-hydrogen atoms. All non-hydrogen atoms were refined with anisotropic displacement parameters and all hydrogen atoms were placed in ideal positions and were refined as riding atoms with individual isotropic displacement parameters.

One of the two $CF_3SO_3^-$ counterions and one of the $(CH_3)_2CO$ molecules exhibit significant translational and torsional rigid-body motion. Modeling the former as a disordered group was considered, but not attempted. Although a TLS rigid body refinement of CF_3SO_3 would yield more realistic results than a disordered refinement, it is doubtful that a significantly better residual would result. The isotropic displacement parameters of the hydrogens on the bridging hydroxyls and on N7′ were tied to 1.2 times that of their host. Drawings of the cation appear in Figures 5 and 8, and selected bond lengths and angles are presented in Table 3. Full details of the structure determination, including tables of bond lengths and angles, atomic positional parameters, and final thermal parameters for non-hydrogen atoms, are given in the supporting information.

$[(L^{iPr_2H}Cu)_2(\mu\text{-}OH)_2](BPh_4)_2\cdot 2THF$. A blue plate crystal of the compound was attached to a glass fiber with heavy-weight oil and mounted on the Siemens SMART system for data collection at 173(2) K. Data collection was performed as described above. Important crystallographic information is given in Table 2. The space group *Cc* was determined based on systematic absences and intensity statistics, which suggested a noncentrosymmetric space group. A successful direct-methods solution was calculated which provided all non-hydrogen atoms from the *E*-map. All non-hydrogen atoms were refined with anisotropic displacement parameters. All hydrogen atoms were placed in idealized positions and refined as riding atoms with individual isotropic displacement parameters.

The unit cell is composed of four dicationic dimers, eight THF solvent molecules, and eight tetraphenylborate anions. The structure solved easily in *Cc*, which presented a model that appeared to be centrosymmetric. The dication, THF molecules, and tetraphenylborate are labeled as though pairs of related atoms pass through a point equidistant from both copper atoms. Attempts to transform one-half of the contents to the centrosymmetric equivalent in space group *C*2/*c* failed. Use of the MISSYM[76] also failed to find any additional symmetry. Therefore, we believe the model presented here to be correct. This specimen desolvated very rapidly to yield crystals with surface fractures. Additionally, the model was refined as a racemic twin in a 66:34 ratio. A thermal ellipsoid drawing of the cation appears in Figure 6, and selected bond lengths and angles are presented in Table 3. Full details of the structure determination, including tables of bond lengths and angles, atomic positional parameters, and final thermal parameters for non-hydrogen atoms, are given in the Supporting Information.

$[(L^{iPr_2Bn}Cu)_2(\mu\text{-}OH)_2](CF_3SO_3)_2$. A blue prism crystal of the compound was mounted on a glass fiber and transferred to an Enraf-Nonius CAD-4 diffractometer with graphite monochromated Mo Kα radiation (λ = 0.710 73 Å). Relevant crystallographic information is given in Table 2. Cell constants and an orientation matrix for data collection were obtained from a least squares refinement of the setting angles for 25 carefully centered reflections in the range $18.12° < 2\theta < 32.05°$. The data were collected at a temperature of 24 ± 1 °C using the ω-2θ scan technique to a maximum 2θ value of 50.1°. An empirical absorption correction was applied (using ψ-scans of three reflections) which resulted in transmission factors ranging from 0.90 to 1.00. The data were corrected for Lorentz and polarization effects; no decay correction was applied.

The structure was solved by direct methods using the TEXSAN software package.[78] Non-hydrogen atoms were refined anisotropically, and the hydrogen atoms were placed at calculated positions. The maximum and minimum peaks on the final difference Fourier map corresponded to 0.56 and −0.66 $e^-/Å^3$, respectively. An ORTEP drawing of the cation appears in Figure 7, and selected bond lengths

(76) PLATON: Spek, A. L. *Acta Crystallogr.* **1990**, *A46*, C34.

(77) SHELXTL V5.0, Siemens Energy & Automation, Inc., Madison, WI 53719-1173.

(78) TEXSAN: Single Crystal Structure Analysis Software, Version 5.0 (1989), Molecular Structure Corporation, The Woodlands, TX 77381.

and angles are presented in Table 3. Full details of the structure determination, including tables of bond lengths and angles, atomic positional parameters, and final thermal parameters for non-hydrogen atoms, are given in the supporting information.

Computational Methods. Anti (C_{2h}) and eclipsed (C_{2v}) conformers of $\{[(NH_3)_3Cu]_2(\mu\text{-}O)_2\}^{2+}$ were fully optimized at the restricted Hartree−Fock (RHF) level of theory using the STO-3G basis set,[79,80] as was a transition state structure that interconnects them via a half-turnstile-like rotation. Analytic frequency calculations verified the nature of these stationary points; frequencies when reported have been scaled by a factor of 0.89.[81] Single-point energies for these three structures were calculated at a variety of levels of theory. Using the STO-3G* basis set, density functional (DFT) calculations were carried out using the local Xα functional[82] and also the gradient corrected exchange and correlation functionals of Becke[83] and Lee−Yang−Parr,[84] respectively (BLYP). To test the stability of the restricted Xα calculation on the eclipsed isomer, a broken-symmetry initial density was constructed by zeroing out all atomic orbital (AO) coefficients associated with one copper atom in the α Kohn−Sham (KS) highest occupied molecular orbital (HOMO), and all AO coefficients associated with the other copper atom in the β KS HOMO. This calculation smoothly converged to the restricted solution.

Additional single-point calculations with the RHF/STO-3G geometries were carried out at the multiconfiguration self-consistent-field (MCSCF) level using the double-ζ polarized basis set of Schafer et al.[85] Nondynamic correlation effects were partially accounted for with a 2-electron/2-orbital (2,2) active space, and additional correlation effects were accounted for using multireference second-order perturbation theory (CASPT2N).[86] For the anti conformer, the active space is formed from molecular orbitals $12a_u$ and $12b_g$; for the eclipsed conformer, the active space is formed from molecular orbitals $13b_1$ and $10a_2$. Geometry optimization at the MCSCF level of theory led to dissociation, suggesting that in the gas phase, the dications are either intrinsically unstable or the calculations require the inclusion of additional correlation to stabilize the $(\mu\text{-}O)_2$ structures. We investigated active spaces up to (8,8) in size, but found dissociation to proceed without barrier in every case; additional electron correlation effects calculated at the CASPT2N level strongly stabilize the $(\mu\text{-}O)_2$ structures relative to the peroxo, but analytic derivatives for this method are not available, and that precludes efficiently accounting for those effects in geometry optimization. Apparently the RHF/STO-3G level serendipitously overstabilizes the complex. Insofar as the RHF/STO-3G structures compare well with experimentally derived structures, we consider it a reasonable approximation to employ these structures for higher level calculations.

The HF and DFT calculations were carried out using the Gaussian94 suite of programs;[87] the MCSCF and CASPT2N calculations were carried out using the MOLCAS suite of programs.[88]

Acknowledgment. We thank the National Institutes of Health (Grant GM47365 to W.B.T., Grant GM33162 to L.Q., and a predoctoral traineeship, Grant GM07323, to E.C.W.), the Searle Scholars Program/Chicago Community Trust (W.B.T.), the National Science Foundation (NYI award to W.B.T., Grant CHE-9525819 to C.J.C., and Grant CHE-9413114 for partial support for the purchase of the Siemens SMART system), the University of Minnesota (dissertation fellowship to J.A.H. and training grants to J.A.H. and S.M. through the Center for Metals in Biocatalysis), and the Alfred P. Sloan and Camille & Henry Dreyfus Foundations (fellowships to W.B.T) for providing funding in support of this research. We are grateful for high-performance vector and parallel computing resources made available by the Minnesota Supercomputer Institute and the University of Minnesota-IBM Shared Research Project, respectively. EXAFS data were collected at the National Synchrotron Light Source (Brookhaven National Laboratory, Beamline X-9A) and the Cornell High Energy Synchrotron Source (CHESS, station C-2). We also thank Professor Kenton Rodgers (North Dakota State University) for assistance with the Raman polarization experiments, Bradley Smith for technical assistance with orbital visualization, Professor Bernt Krebs (Münster, FRG) for supplying the coordinates for the X-ray structure described in ref 3d, and Professor Holden H. Thorp (University of North Carolina) for helpful discussions.

Supporting Information Available: Complete drawings and full details of the X-ray structure determinations, including tables of bond lengths and angles, atomic positional parameters, and final thermal parameters (66 pages). See any current masthead page for ordering and Internet access instructions.

JA962305C

(79) Hehre, W. H.; Stewart, R. F.; Pople, J. A. *J. Chem. Phys.* **1969**, *51*, 2657.

(80) Pietro, W. J.; Hehre, W. J. *J. Comput. Chem.* **1983**, *4*, 241.

(81) Pople, J. A.; Scott, A. P.; Wong, M. W.; Radom, L. *Isr. J. Chem.* **1993**, *33*, 345.

(82) Slater, J. C. *Phys. Rev.* **1951**, *81*, 385.

(83) Becke, A. D. *Phys. Rev. A* **1988**, *38*, 3098.

(84) Lee, C.; Yang, W.; Parr, R. G. *Phys. Rev. B* **1988**, *37*, 785.

(85) Schafer, A.; Horn, H.; Ahlrichs, R. *J. Chem. Phys.* **1992**, *97*, 2571.

(86) (a) Andersson, K.; Malmqvist, P.-Å.; Roos, B. O.; Sadlej, A. J.; Wolinski, K. *J. Phys. Chem.* **1990**, *94*, 5483. (b) Andersson, K.; Malmqvist, P.-Å.; Roos, B. O. *J. Chem. Phys.* **1992**, *96*, 1218. (c) Andersson, K.; Roos, B. O. *Int. J. Quant. Chem.* **1993**, *45*, 591.

(87) Frisch, M. J.; Trucks, G. W.; Schlegel, H. B.; Gill, P. M. W.; Johnson, B. G.; Robb, M. A.; Cheeseman, J. R.; Keith, T.; Petersson, G. A.; Montgomery, J. A.; Raghavachari, K.; Al-Laham, M. A.; Zakrzewski, V. G.; Ortiz, J. V.; Foresman, J. B.; Cioslowski, J.; Stefanov, B. B.; Nanayakkara, A.; Challacombe, M.; Peng, C. Y.; Ayala, P. Y.; Chen, W.; Wong, M. W.; Andres, J. L.; Replogle, E. S.; Gomperts, R.; Martin, R. L.; Fox, D. J.; Binkley, J. S.; Defrees, D. J.; Baker, J.; Stewart, J. P.; Head-Gordon, M.; Gonzalez, C.; Pople, J. A. *Gaussian 94 RevC.1*; Gaussian Inc.: Pittsburgh, PA, 1995.

(88) Andersson, K.; Blomberg, M. R. A.; Fülscher, M. P.; Karlström, G.; Kellö, V.; Lindh, R.; Malmqvist, P.-Å.; Noga, J.; Olsen, J.; Roos, B. O.; Sadlej, A. J.; Siegbahn, P. E. M.; Urban, M.; Widmark, P.-O. *MOLCAS-3*; University of Lund: Sweden, 1994.